LUND UNIVERSITY

Master of Science Thesis
VT2015

Flattening filter free volumetric modulated arc therapy for extreme hypo-fractionation of prostate cancer - Decreasing the treatment time and reducing the impact of prostate motion

Minna Ahlström

Supervision

Hunor Benedek, Per Nilsson, Tommy Knöös and Crister Ceberg, Lund

Department of Medical Radiation Physics,
Clinical Sciences, Lund
Lund University
www.msf.lu.se

ABSTRACT

Purpose: To examine the feasibility of flattening filter free (FFF) volumetric modulated arc therapy (VMAT) for extreme hypofractionation of prostate cancer and investigate the potential decrease in treatment time per fraction while preserving or improving the treatment quality. To investigate the impact of intrafractional prostatic displacement.

Material and methods: Single arc treatment plans with photon beam qualities 10 MV with flattening filter (FF), 6 MV FFF and 10 MV FFF were created for nine patients treated with conventional fractionation (78 Gy, 2 Gy/fraction) and hypofractionation (42.7 Gy, 6.1 Gy/fraction), respectively. Dose-volume histograms (DVH) for all beam qualities were statistically evaluated using a paired sample Student's t-test. Treatment delivery was evaluated through measurements on a Varian TrueBeam™ using a Delta4 PT system (ScandiDos AB). The beam-on time for each plan was recorded. A motion study, including one FF and one FFF hypofractionated treatment plan, was also performed using the HexaMotion (ScandiDos AB) and with trajectory data from six authentic prostate movement patterns.

Results: All treatment plans were approved by a senior radiation oncologist. Evaluating the DVHs, no significant differences between beam qualities or between fractionation schedules were observed. All objectives were met for all plans. At the treatment delivery all plans passed the gamma criterion 3%, 2 mm with a pass rate of 98.8% or higher. The beam-on time for all conventional treatment plans was 1.0 minute. The mean beam-on time was 2.3 minutes for the hypofractionated 10 MV FF plan, 1.3 minutes for the 6 MV FFF and 1.0 minute for the 10 MV FFF. In the motion study, no or little effect was observed on the pass rate for displacements ≤1mm. The shorter treatment delivery was superior for three patterns, while the longer treatment was preferred in the case of temporal displacement of the prostate.

Conclusions: The treatment time for extreme hypofractionation of prostate cancer is reduced to less than half the time per fraction by combining FFF-technique with VMAT. The treatment plan quality was preserved for the FFF beams. Finally, a shorter beam-on time also seems advantageous for the majority of prostate motion patterns investigated. Based on this work, it is feasible to implement FFF VMAT for extreme hypofractionation of prostate cancer (HYPO-RT-PC trial) at the radiotherapy department at Skåne University Hospital, Lund.

Popular scientific summary in Swedish:

Snabb, säker och strålande – ny teknik vid behandling av prostatacancer

I skrivande stund är sju olika cancercentra i Sverige, däribland Skånes Universitetssjukhus i Lund, mitt uppe i en gemensam randomiserad studie som undersöker behandling av prostatacancer med två olika strålningsscheman. Patienterna i studien blir slumpvis tilldelade antingen en standardbehandling, där de får en liten mängd strålning vid 39 olika tillfällen, eller en så kallad hypofraktionerad behandling, där de istället får ca tre gånger så mycket strålning per gång vid endast 7 tillfällen. Målet med studien är att testa om den hypofraktionerade behandlingen kan ge ett bättre resultat med ökad bot utan högre grad av biverkningar.

Prostatacancer är den vanligaste cancerformen i Sverige och årligen diagnosticeras nära 10 000 män – motsvarande ungefär en man i timmen, dygnet runt, året om. Prostatan i sig är en körtel som sitter i nedre delen av buken, nära blåsa och ändtarm. Eftersom den inte är fixerad i någon fast struktur påverkas prostatans position av bland annat blåsfyllnad, ändtarms-aktivitet och ofrivilliga muskelrörelser i underkroppen. Detta innebär att prostatan även har en viss sannolikhet att röra sig under pågående strålbehandling, trots att positionen verifieras och, vid behov, justeras genom bildtagning innan varje behandling påbörjas. Studier har visat att avvikelsen i prostatans position blir större ju längre tid som går, varför många menar på att man bör hålla behandlingstiderna så korta som möjligt. Eftersom det vid hypofraktionering tar längre tid vid varje behandlingstillfälle, då en större mängd strålning ska levereras, har syftet med detta examensarbete varit att undersöka hur mycket behandlingstiden kan förkortas genom användning av en nyare teknik, så kallad flattening filter free (FFF) strålbehandling. Målet var även att säkerställa att de nya behandlingarna kunde planeras och levereras med minst lika bra kvalitet som de nuvarande. För detta valdes nio patienter ut från hypo-studien och jämfördes på sex olika sätt. Slutligen genomfördes en rörelsestudie på en av patienterna, där några olika rörelsemönster och deras eventuella inverkan på strålleveransens precision undersöktes.

Resultaten visade att genom att kombinera FFF-teknik med den redan befintliga rotations-behandlingen, kunde tiderna för hypofraktioneringen mer än halveras för samtliga patienter. Efter noggrann utvärdering av behandlingsplanerna genererade med FFF, kunde dessa konstateras hålla samma höga kvalitet som de med nuvarande teknik. Vidare kunde även en högkvalitativ strålleverans säkerställas genom inmätning med kvalitetssäkringsutrustning. Den nya, korta behandlingstiden är densamma som för en standardbehandling, samtidigt som tre gånger mer strålning levereras. Med hypofraktionering behöver patienten bara behandlas vid 7 tillfällen, jämfört med annars 39, vilket gynnar både den individuella patienten men också sjukvården och samhället i stort, sett ur ett ekonomiskt perspektiv. Fördelen med att hålla nere tiden visade sig även i rörelsestudien, där en kort behandling gav bättre resultat än en lång för alla undersökta rörelsemönster utom ett, men där var skillnaden väldigt liten. Det var tydligt att prostatans drift ur position påverkade strålleveransen, även inom tidsramen av några få minuter.

Baserat på detta arbete kunde slutsatsen dras att det är möjligt, och dessutom fördelaktigt, att minska behandlingstiden för hypofraktionerad strålbehandling av prostatacancer, genom införandet av FFF-teknik, ner till samma tid som det tar att leverera en standardbehandling.

Minna Ahlström

Handledare: Hunor Benedek, Per Nilsson, Tommy Knöös och Crister Ceberg
Examensarbete (30 hp) i medicinsk strålningsfysik, vårterminen 2015
Avdelningen för medicinsk strålningsfysik, Lunds Universitet
Strålningsfysik, Skånes universitetssjukhus, Lund

ACKNOWLEDGMENTS

First of all, I would like to thank my supervisors:

Hunor Benedek, thank you for setting up the project and giving me the opportunity to work with you. Thank you for always motivating and inspiring me.

Per Nilsson, thank you for always making time for me and for sharing your endless knowledge in the field. Thank you for believing in me.

Tommy Knöös and Crister Ceberg, thank you for your inputs and feedback, always helping me improve my work.

A special mention also to:

Paul Keall and Jin Ng, thank you for sharing your prostate trajectory data, adding valuable results.

ScandiDos AB, thank you for your excellent support and great patience in our last minute attempt to set up the Delta^{4DVH} Anatomy module.

André Haraldsson, thank you for sharing your expertise in the field of treatment planning.

Fredrik Nordström, thank you for sharing your C# code.

I would also like to thank my fellow students **Rrezarta** and **Emilia** for four amazing years together and for making this final half a year the best one yet. I will miss you both!

Finally, I would like to thank my family and friends for all your love and support. I would not be where I am today without you.

Minna Ahlström
Lund, May 22nd 2015

ABBREVIATIONS AND ACRONYMS

AAA	Analytical Anisotropic Algorithm
AP	Anterior-Posterior
BED	Biological Effective Dose
CT	Computed Tomography
CTV	Clinical Target Volume
DVH	Dose-Volume Histogram
FFF	Flattening Filter Free
IGRT	Image Guided Radiation Therapy
IMRT	Intensity Modulated Arc Therapy
MLC	Multi-Leaf Collimator
MU	Monitor Unit
OAR	Organs at Risk
PC	Prostate Cancer
PTV	Planning Target Volume
RT	Radiation Therapy
SI	Superior-Inferior
TPS	Treatment Planning System
VMAT	Volume Modulated Arc Therapy

TABLE OF CONTENTS

1 INTRODUCTION

Radiotherapy is a treatment given to about 45-55 % of all cancer patients in Europe (Slotman et al., 2005). External beam radiotherapy (EBRT) is a non-invasive treatment with the aim to accurately deliver a high radiation dose to the tumour while preserving the surrounding normal tissues. Recent decades' of technical and computational evolution has allowed for more advanced treatment techniques to become widely available. Since the first medical linear accelerator in 1953, the treatments as well as the radiation beams have become increasingly complex (Thariat et al., 2013). In the mid 90's Yu (1995) presented intensity modulated arc therapy (IMAT), a rotational therapy continuously modulating the beam, at a fixed dose rate and gantry rotation speed, using several overlapping arcs. Otto (2008) further refined this technique and introduced the volumetric modulated arc therapy (VMAT) technique, where the aim was to deliver optimized treatment plans with high dose conformity in an efficient and accurate way. The VMAT technique allows beam-on during a full gantry rotation of 360° with simultaneous modulation of the multileaf collimator (MLC) and a variation of gantry rotation speed as well as dose rate. VMAT can be used for treating various types of cancer and is for example the most efficient radiotherapy for prostate cancer, delivering high quality treatments in the least amount of time (Wolff et al., 2009).

Prostate cancer is the most common type of cancer in Sweden. During 2012 almost 9000 men were diagnosed with the disease. In the past 20 years there has been an increasing incidence, mainly due to diagnostics using PSA-testing but also as a result of an older population (Cancerfonden, 2014). For localized prostate cancer, the disease is divided into three categories; low risk, intermediate risk and high risk (Swedish national health care programme for prostate cancer, 2015). The choice of treatment is based on the severity of the cancer, with the following options; to monitor the patient with no treatment (watchful waiting), surgery or radiation therapy. Some patients are prescribed a combination of treatments and others may also receive hormone therapy. According to an evidence based estimate from 2003, about 60 % of the prostate cancer patients will require radiotherapy at some point during their illness, including palliative treatment (Foroudi et al., 2003).

There is an on-going debate about the radiobiology of prostate cancer, affecting the choice of optimal fractionation schedule in the treatment of the cancer where, typically, radiation fraction sizes of 1.8 to 2.0 Gy have been used as standard (Nahum, 2015). The Biologically Effective Dose (BED) depends not only on the total dose (D) given but also on the dose per fraction (d). The model for calculating BED is based on the linear quadratic model for cell survival; $S = e^{-D(\alpha+\beta d)}$. The ratio α/β quantifies the fractionation sensitivity of the tissue. Recent studies imply that the α/β ratio for prostate cancer is lower than previously assumed (Williams et al., 2007, Brenner and Hall, 1999), and even lower than for late normal tissue complications, which indicates a potential benefit of using hypofractionated radiotherapy. If α/β is low, the cancer cells would be more sensitive to large fraction sizes; thus hypo-fractionation, delivering higher absorbed dose per fraction using fewer fractions, may be favourable.

A current Scandinavian study by Widmark et al. (2014) is investigating this issue. The study is a prospective randomized phase III trial (HYPO-RT-PC), which compares extreme hypofractionation with conventional fractionation in intermediate risk prostate cancer patients. One of the major recruiting trial centres is Skåne University Hospital in Lund (SUS). In the study the patients are randomly assigned to a conventional treatment, 78 Gy in 39 fractions (2.0 Gy/fr), or to a hypo-fractionated treatment, 42.7 Gy in 7 fractions (6.1 Gy/fr). This extreme version of hypofractionation is advantageous based on theoretical improvements in outcome, without increasing late toxicity. The treatment is delivered via image-guided radiotherapy (IGRT) where daily kilo voltage (kV) set-up images or cone beam computed tomography (CBCT) is used to verify the position of the prostate based on implanted fiducial markers. In Lund the treatment is delivered using VMAT with daily kV set-up images.

As a result of the higher fraction dose of the hypofractionated treatment, each treatment session will consequently have a longer duration compared to the conventionally fractionated treatment. The

longer the session, the less accurate is the position of the patient (and the prostate gland in particular). The prostate gland is not attached to any fixed anatomical structure and could thus move inter- and intra-fractionally. Any change in position of the prostate between fractions can be corrected for using IGRT. The movement within a fraction is more complex, where any displacement of the prostate during treatment is likely to be due to rectal movements, muscle clenching or leg movement (Nederveen et al., 2002). The majority of prostate movements are accounted for in the added margin when outlining the target prior to the treatment. However, temporary displacements where the prostate gland has moved more than 10 mm for part of the fraction have been reported (Padhani et al., 1999). This could potentially lead to less dose coverage, especially in the case of hypofractionation. Tong et al. (2015) and Ballhausen et al. (2015) have recently emphasised the importance of keeping the treatment times to a minimum because of uncertainties due to prostate motion.

A faster radiation delivery can be achieved using flattening filter free (FFF) photon beams. Removing the flattening filter allow for a significant increase in dose rate, which ultimately can shorten the treatment times (Gasic et al., 2014, Alongi et al., 2013, Dzierma et al., 2014).

2 AIM

The purpose of this study was to investigate the potential saving in treatment time for VMAT with flattening filter free photon beams in extremely hypofractionated radiotherapy of prostate cancer, and especially for the HYPO-RT-PC study. The goal was to decrease the treatment delivery time per fraction, while preserving or improving the treatment plan quality. Radiation delivery quality was verified through measurements. The analysis was carried out as a treatment planning study on nine patients from the HYPO-RT-PC study. Six different treatment plans were designed and evaluated for each patient.

A review was also carried out on the currently available literature on prostate motion in order to discuss the clinical importance of shortening the treatment session. A motion study was designed for six different prostate trajectories (Ng et al., 2012), where the two most extreme treatment plans for a selected patient were delivered during motion. The aim was to get an indication of the impact of different prostate motion patterns and identify any differences between the treatments with flattened and unflattened beams.

3 THEORY AND BACKGROUND

3.1 VMAT

Volumetric modulated arc therapy (VMAT) is a novel radiotherapy technique. It can typically deliver a 2 Gy fraction with high dose conformity to the target while preserving the healthy surrounding tissue, all in less than 2 minutes (Palma et al., 2010). The high accuracy of the treatment is achieved using inversely optimized treatment planning. Varian Medical System has termed their VMAT technique RapidArc®, which entered the market in 2008. In the radiotherapy department at the Skåne University Hospital there are currently six Varian TrueBeam™, all equipped with VMAT. The outputs of the linacs are matched and verified on a regular basis, providing equivalent treatment deliveries. The measurements of this study were carried out on one of the TrueBeams, while the results are assumed to be valid for all of them.

The idea behind VMAT is developed from intensity modulated arc therapy. The algorithm optimizing the treatment plan allows the dose to be delivered during a full 360° rotation of the gantry. The technological requirement is a rotational medical linear accelerator equipped with a dynamic multileaf collimator (MLC), the possibility to vary dose rate and a gantry rotation speed that can be adjusted accordingly (Otto, 2008).

3.1.1 OPTIMIZATION OF TREATMENT PLANS

The VMAT optimization algorithm integrates the MLC position and the monitor unit (MU) weight as its parameters. In the process, both mechanical and efficiency constraints are applied. The goal function that determines the outcome of a performed iteration is based on dose-volume objectives. These are defined individually by the user who may put constraints on both upper and lower absorbed doses to the tumour as well as upper dose constraints to surrounding organs. Over the iterations the goal function is optimized towards its minimum. The duration of the process is determined by a defined stopping criteria or by a maximum number of iterations.

VMAT optimization operates on the idea of a finite number of static positions used to simulate the dynamic motion. The full arc is divided into ten initial positions, evenly distributed over the range of angles. Midway between each of these consecutive samples, a MLC instantaneous configuration is modelled and the MU weight is averaged over the covered sub-arc angle range. This is the starting position of the inverse optimization process. Using several iterations, both MLC positions and MU deliveries are optimized. Next, new sample points are added between each of the ten initial samples as the optimization continues (see Figure 1 for illustration). Each time a new sample is introduced, the goal function is recalculated. The process is repeated until the desired sampling frequency is reached. Unsurprisingly, the higher the sampling frequency, the more accurate the estimation of the delivered plan will become (Otto, 2008).

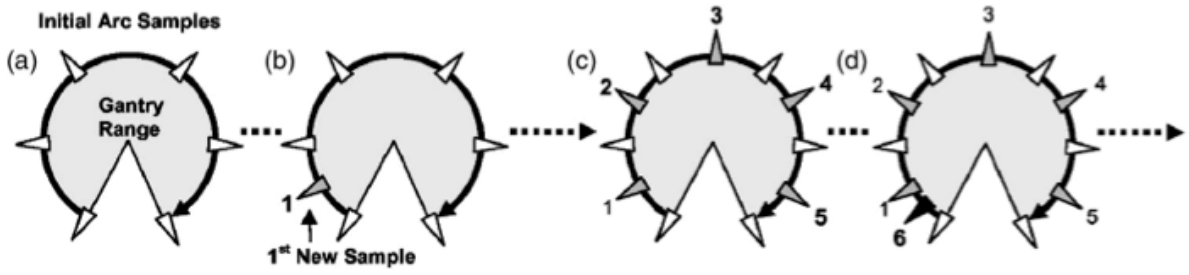

Figure 1. (a) The optimization is initially based on a small set of static points.
(b, c) New sample points are successively added between the already existing control points.
(d) The process is repeated until the desired frequency of control points is reached. (Otto, 2008)

The VMAT plans in this study were created in the Eclipse treatment planning system (Varian Medical Systems, Inc.) using its VMAT optimizer. Different weight factors are set to different structures, based on the priorities of the constraints (usually defined in a separate treatment protocol). Objectives can also be changed interactively throughout the optimization. The optimization process itself is based on the one described above and is a progressive resolution optimization. For VMAT the process is divided into 4 multi-resolution (MR) levels, where control points are added in groups instead of one at a time. The initial number of control points is 10 and increases at the end of every MR, reaching 178 control points at MR4.

3.1.2 DOSE CALCULATION

For absorbed dose calculations in Eclipse the Anisotropic Analytical Algorithm (AAA) for photons is applied. The algorithm is based on a three dimensional pencil beam convolution/superposition with a possible grid range of 1-5 mm. The calculation accounts for heterogeneities inside the patient's body, through photon scatter kernels. These are weighted by information from the patient's CT image sets, working both in the beam's direction as well as perpendicular to it. The configuration of photon beams is modelled from separate Monte Carlo simulations for the primary photon beam, scattered photons and electrons scattered from the treatment head. The final dose volume is calculated with photon and electron convolutions that are super-positioned (Varian Medical Systems, 2011). In this study the AAA version 10.0.28 was used with a grid size of 2.5 mm.

The AAA has been shown to produce accurate dose modelling not only for standard photon beams but also for FFF beams (Lang et al., 2012).

3.2 PLAN COMPLEXITY

Treatment plans can express different levels of delivery complexity. In this study the complexity is measured in monitor units (MU) per unit dose (Gy). A standard open field of 10 cm x 10 cm requires, by definition, 100 MU to deliver 1 Gy at the depth of maximum dose and SSD = 100 cm. The definition of MU is the same for all beam qualities, allowing relative comparison between energies. An open field has no modulation and thus the lowest grade of complexity. A treatment plan that requires a larger number of MU to fulfil the dose constraints, for a set prescribed dose, is said to be more complex. In general, a plan that is more modulated automatically uses a larger number of MU. One reason for this can be contradictory constraints on the defined target and nearby organs at risk (OAR). In the case of prostate cancer this can occur because of the requirements on dose coverage of the prostate (target) and the request to keep rectum dose to a minimum.

Effectively, the complexity is reflected in the MLC-movement pattern. To deliver a more complex plan, the MLC must move more rapidly and the shift in MLC position of individual leafs is likely to be larger between two control points. The complexity could also affect the dose rate. If the modulation is too complex, the gantry speed is reduced in order to deliver the required dose in a segment. This could lead to an increase in treatment time, which contradicts the purpose of VMAT being the most efficient treatment technique. Other measures of complexity are also available, but for the purpose of this work the concept of MU/Gy was considered sufficient.

3.3 HYPOFRACTIONATED RADIOTHERAPY

During the last decades, conventionally fractionated dose escalation has been a major trend in radiotherapy of prostate cancer. It has shown to improve biochemical control without significant increase in late toxicity (Hall and Giaccia, 2006). However, recent studies imply that the radiobiological properties of the prostate cancer cells are more similar to late-responding normal tissues than acutely reacting tissues and several other tumours. This suggests that the tumour control could be equally good or improved, without increased toxicity, choosing a treatment schedule with fewer but larger fractions (Williams et al., 2007, Brenner and Hall, 1999). Radiotherapy schedules using less number of fractions prescribed with a higher dose (>2 Gy) in each fraction are called hypo-fractionated regimens.

3.3.1 BIOLOGICALLY EFFECTIVE DOSE AND THE LINEAR-QUADRATIC CONCEPT

The linear quadratic model is often used to compare different fractionation schedules in a quantitative way. Through this model the biological effective dose (BED), as a function of prescribed dose and number of fractions, may be calculated. The model also includes a radiobiological constant (α/β) representing the type of radiation damage, acute or late. Acute normal tissue reactions are by definition those that appear during treatment or within 90 days after finishing the treatment, while late damage appears more than 90 days after finishing the treatment.

The linear quadratic model is based on the cell-survival curve, survival as a function of absorbed dose (Figure 2). The curve has an initial slope followed by a shoulder, which depends on the accumulation and ability to repair sublethal damage of the cells. No shoulder indicates the lack of ability to repair cells. The cell survival at a delivered single dose, D, may thus be expressed as

$$S = e^{-\alpha D - \beta D^2} \quad \textbf{(1)}$$

where α is the $\log_e$ of the cells killed per gray (the linear component) and β is the $\log_e$ of the cells killed per gray squared. The cell killing due to the linear and the quadratic components, respectively, are equal at dose $D = \alpha/\beta$.

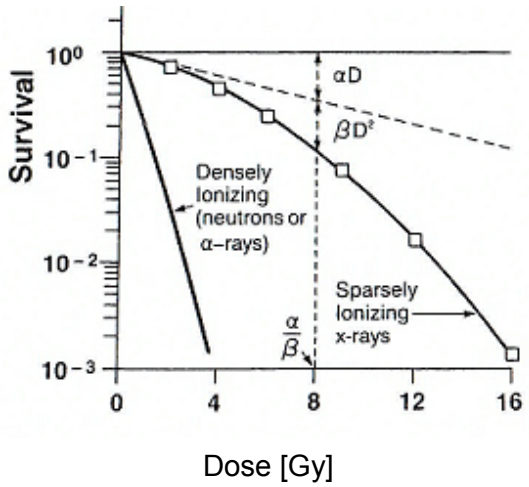

Figure 2. Graph illustrating the linear-quadratic relation between radiation cell survival, *S*, and dose, *D*. For densely ionizing radiation the cell survival is an exponential function of the dose, $S=\exp(-\alpha D)$. For sparsely ionizing radiation, such as x-rays, the curve has an initial slope, followed by a shoulder and includes a linear and a quadratic component, $S=\exp(-\alpha D-\beta D^2)$. The two components are equal at dose $D=\alpha/\beta$. (Chul-Seung and Young-Nam, 2013)

The biological effect of a single fraction of dose, D, is assumed to be proportional to –ln(S) and is hence given by

$$E = \alpha D + \beta D^2 \quad \textbf{(2)}$$

For n fractions of dose d the biological effect may be expressed as

$$E = n(\alpha d + \beta d^2) \quad \textbf{(3)}$$

assuming the time between fractions is long enough for complete repair of sublethal damage between fractions. Finally, biological effective dose (BED) is the quantity of which different fractionation regimens are compared. This is expressed as E divided by α and then rearranged, giving

$$BED = \frac{E}{\alpha} = (nd) \times \left(1 + \frac{d}{\alpha/\beta}\right) = (\text{total dose}) \times (\text{relative effectiveness}) \quad \textbf{(4)}$$

The α/β ratio can be interpreted as a quantification of the fractionation sensitivity of the tissue. A low α/β indicates a larger sensitivity to changes in fractionation size and is found in e.g. late-responding tissues. Early-responding tissues are often assigned a larger α/β, indicating less sensitivity to fractionation changes (Hall and Giaccia, 2006).

The effect of a given treatment schedule can be converted to that of a standard schedule of 2 Gy per fraction using the equivalent dose, EQD2. This is derived from the respective BED equations provided that α/β is equal in the two regimens. The equivalent dose of the arbitrary schedule then becomes

$$EQD2 = D \cdot \frac{d+\alpha/\beta}{2+\alpha/\beta} \quad \textbf{(5)}$$

where D is the total dose and d is the fraction dose, both of the arbitrary schedule.

In the HYPO-RT-PC study the standard fractionated treatment delivers a total of 78 Gy in 2 Gy fractions to the PTV, whereas the hypofractionated treatment delivers 42.7 Gy in 6.1 Gy fractions. Performing the calculation of EQD2 on the schedule of the hypofractionated treatment arm yields the following results:

$$\alpha/\beta = 3 \text{ Gy} \rightarrow EQD2 = 78 \text{ Gy}$$
$$\alpha/\beta = 1.5 \text{ Gy} \rightarrow EQD2 = 93 \text{ Gy}$$

Hence, the hypofractionated treatment is equally efficient to the standard treatment if α/β=3 Gy (typical α/β ratio for late normal tissue reactions) but is theoretically superior to the standard treatment if α/β=1.5 Gy, as recent publications indicate (Dasu and Toma-Dasu, 2012).

3.4 FLATTENING FILTER FREE X-RAY BEAMS

The flattening filter is a standard component in the treatment head of medical linear accelerators. The cone-shaped filter flattens the x-ray dose profile and creates a uniform beam (Metcalfe et al., 2007). However, as the treatment techniques have become more advanced and modalities such as intensity modulated rotational therapy (IMRT) and VMAT have been introduced, the flat beam profile is no longer an obvious requirement, and removing the flattening filter may even be favourable in specific situations (Stathakis et al., 2009, Gasic et al., 2014).

When removing the flattening filter, the beam characteristics change. The profile of the FFF beam becomes conical and has a softer spectrum. The effect of off-axis softening, seen in flattened beams, is not as significant in unflattened beams. Due to the reduction of this effect the depth dose

characteristics are almost constant throughout the entire field. This is also observed in that the shape of the dose profile with depth changes less than for flattened beams (by only a few percentage units) (Georg et al., 2011). Further, there is less head scatter when the flattening filter, being one of the main sources of scatter, is removed which might reduce the relative risk of out-of-field secondary malignancies (Murray et al., 2015). Finally, the fact that the maximum available dose rate is at least double the one in flattened beams is beneficial in reducing the duration of the treatment delivery (Dzierma et al., 2014).

3.5 DELTA^4 AND HEXAMOTION

The Delta^4 pre-treatment verification phantom is a product from ScandiDos AB, Uppsala, Sweden. The phantom can be used for verifications of advanced radiotherapy treatment techniques, such as VMAT. Studies have shown that the reproducibility of the measurements is high on a day-to-day basis as well as for repeated measurements (Korreman et al., 2009). The Delta^4 has also been proven equally successful for dose evaluation using high dose rate FFF beams in VMAT, where the introduced dose difference between high and low dose rates was shown to be negligible (Kalantzis et al., 2012).

The phantom is an acrylic (Polymethylmethacrylate, PMMA) cylinder with two integrated, orthogonally positioned, detector planes. Each detector plane has a detection area of 200x200 mm^2, with a total of 1069 p-type Si detectors. The positioning of the detector elements is particularly dense, with a resolution of 5 mm, around the isocenter which allows for accurate measurements of the dose distribution in this region, making the phantom a suitable tool for complex plan evaluation.

The Hexamotion is a supplementary module from ScandiDos, which can be used in combination with the Delta^4 to simulate multi-dimensional realistic movement patterns. A text file describing the trajectory of the phantom motion in three dimensions is used as input. The frequency of position changes is 50 Hz, with a guaranteed accuracy in position of at least 0.5 mm (ScandiDos AB, Uppsala, 2012).

3.6 DOSE DISTRIBUTIONS AND GAMMA EVALUATION

The comparison of planned and delivered dose is often analysed with three different methods; distance to agreement (DTA), dose deviation and gamma index.

The basic idea of the dose deviation is to calculate the difference between the measured D_m and the calculated dose D for every position, $\boldsymbol{r}$. The dose deviation is most suitable in regions with low dose gradients. In areas of high dose gradients a small offset in position may result in large, not necessarily relevant, dose deviations. Therefore, in areas of high dose gradients the method of distance-to-agreement (DTA) is more applicable. This method also compares two dose distributions, but for every point in the measured data, the nearest point in the calculated data with the same dose as the measured point is identified. The distance between the two points is calculated and defined as the DTA. Both methods are supplemented by acceptance criteria set by the user aiming to identify areas of significant disagreement.

Gamma evaluation was established by Low et al. (1998) as a numerical quality index for evaluation of three-dimensional (3D) treatment planning systems. Their aim was to combine the already existing methods of dose deviation and distance to agreement (DTA), and present a more instructive evaluation method to display the areas that fail both comparison criteria.

The gamma criterion can be represented by an ellipsoid in a coordinate system representing space and dose simultaneously (Figure 3). Assuming that the dose-deviation criterion is defined as ΔD_M

(e.g. 3%) and the DTA criterion is Δd_M (e.g. 2 mm), the gamma acceptance criterion can be defined as the ellipsoid surface represented by the two methods simultaneously:

$$1 = \sqrt{\frac{r^2(\boldsymbol{r}_m,\boldsymbol{r})}{\Delta d_M^2} + \frac{\delta^2(\boldsymbol{r}_m,\boldsymbol{r})}{\Delta D_M^2}} \quad \textbf{(6)}$$

where the DTA and the dose difference are mathematically described as

$$r(\boldsymbol{r}_m,\boldsymbol{r}) = |\boldsymbol{r} - \boldsymbol{r}_m| \quad \textbf{(7)}$$

and

$$\delta(\boldsymbol{r}_m,\boldsymbol{r}) = D(\boldsymbol{r}) - D_m(\boldsymbol{r}_m) \quad \textbf{(8)}$$

where $\boldsymbol{r}_\mathrm{m}$ is the position of the measured data point and $\boldsymbol{r}$ is an arbitrary position of comparison.

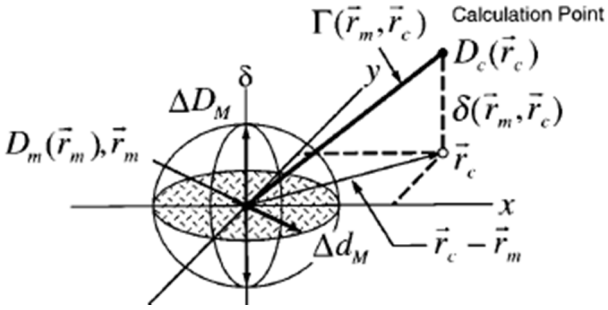

Figure 3. Two-dimensional geometric representation of the ellipsoid representing the combined evaluation of dose difference and distance-to-agreement. The measured data point is located at the origin of the coordinate system (Low et al., 1998).

The gamma index is identified as the difference in dose distributions between the calculated and the measured doses. For each measured point in the evaluation a gamma value is determined for every calculated point according to:

$$\Gamma(\boldsymbol{r}_m,\boldsymbol{r}_c) = \sqrt{\frac{r^2(\boldsymbol{r}_m,\boldsymbol{r_c})}{\Delta d_M^2} + \frac{\delta^2(\boldsymbol{r}_m,\boldsymbol{r_c})}{\Delta D_M^2}} \quad \textbf{(9)}$$

where

$$r(\boldsymbol{r}_m,\boldsymbol{r_c}) = |\boldsymbol{r_c} - \boldsymbol{r}_m| \quad \textbf{(10)}$$

and

$$\delta(\boldsymbol{r}_m,\boldsymbol{r_c}) = D_c(\boldsymbol{r_c}) - D_m(\boldsymbol{r}_m) \quad \textbf{(11)}$$

where $\boldsymbol{r}_\mathrm{c}$ is the position of the calculated dose, which is to be compared to the measured dose in $\boldsymbol{r}_\mathrm{m}$.

The gamma index is defined as the smallest gamma value:

$$\gamma(\boldsymbol{r}_m) = \min\{\Gamma(\boldsymbol{r}_m,\boldsymbol{r})\}\,\forall\{\boldsymbol{r}_c\} \quad \textbf{(12)}$$

The result of the evaluation is determined by the outcome of the gamma index. A point passes the gamma criterion if $\gamma(\boldsymbol{r}_m) \leq 1$, whereas a point fails if $\gamma(\boldsymbol{r}_m) > 1$.

3.7 PROSTATE MOTION

Image guided radiotherapy has reduced the uncertainty of inter-fractional motion of the prostate gland. Verification of the prostate position within the pelvis relative to bony structures or through implanted markers at the start of each treatment session has improved the outcome of the radiotherapy (Zelefsky et al., 2012). However, rectal activity, bladder filling, muscle clenching and pelvis movements, all of which may occur during the course of a single treatment fraction, also affect the position of the prostate and could potentially induce prostate displacement and changes in prostate shape during the treatment fraction (Nederveen et al., 2002). The intra-fractional prostatic motion adds uncertainty to the position and must be accounted for in added CTV-PTV margins in order to minimise the risk of reduced target coverage. There are numerous studies investigating the issue of prostate displacement, using various techniques such as cine MRI, ultrasound, electromagnetic markers, on-line x-ray images and continuous monitoring using a radiofrequency tracking system. For this section, some of the currently available literature on intra-fractional motion has been selected and studied. A summary is presented in Table 3.1.

3.7.1 INTRA-FRACTIONAL MOTION

Intra-fraction prostate motion studied using pre- and post-treatment imaging is reported by e.g. Gladwish et al. (2014) and Quon et al. (2012). These studies investigate hypofractionated VMAT treatments of prostate cancer with fractionation schedules of 40 Gy in 5 fractions and 35 Gy in 5 fractions, respectively. The mean 3D displacement of the prostate during treatment sessions of 195±59 seconds is reported as 2.32±1.55 mm by Gladwish et al. (2014). They report 3D prostate displacements larger than 5 mm in 4% of the fractions. In the study by Quan et al. (2012), the prostate had a 3D displacement larger than 5 mm in 14% of the fractions. The part of the total treatment where the individual patient exhibited large prostate displacement was between 0-80% of the fractions. Due to the inter-patient variations they suggest that patients with large prostate motion are identified and given an individualised treatment with increased margins or other interventions. Both studies do conclude that prostate motion stays small in general. A limitation to studies based on only pre- and post-treatment images, is that any temporal prostate displacements are undetectable.

Many studies have used real-time monitoring with different techniques to study the intra-fractional prostate motion. In this way, temporal displacements are not omitted and the actual motion pattern of the prostate may be mapped.

In a study by Ng et al. (2012) ten patients were monitored in a total of 268 fractions using kilovoltage intrafraction monitoring (KIM) providing a 3D position of the prostate. They report six different types of prostate trajectories; stable target position, continuous drift, transient excursion, persistent excursion, high-frequency excursions and erratic behaviour (Figure 4). One patient exhibited 3D prostate displacement larger than 15 mm, where the persistent excursion (Figure 4 D) is an indication of a large uncorrected geometric miss (Ng et al., 2012). In general the observed motion was small, where 3D displacement larger than 3 mm was observed in only 4.7% of the cases. Kupelian et al. (2007) report similar motion patterns using the Calypso 4D localization system (Varian). In their study, a much higher incidence rate of prostate displacements were observed. Displacements > 3 mm for at least 30 cumulative seconds were reported in 41% of the fractions.

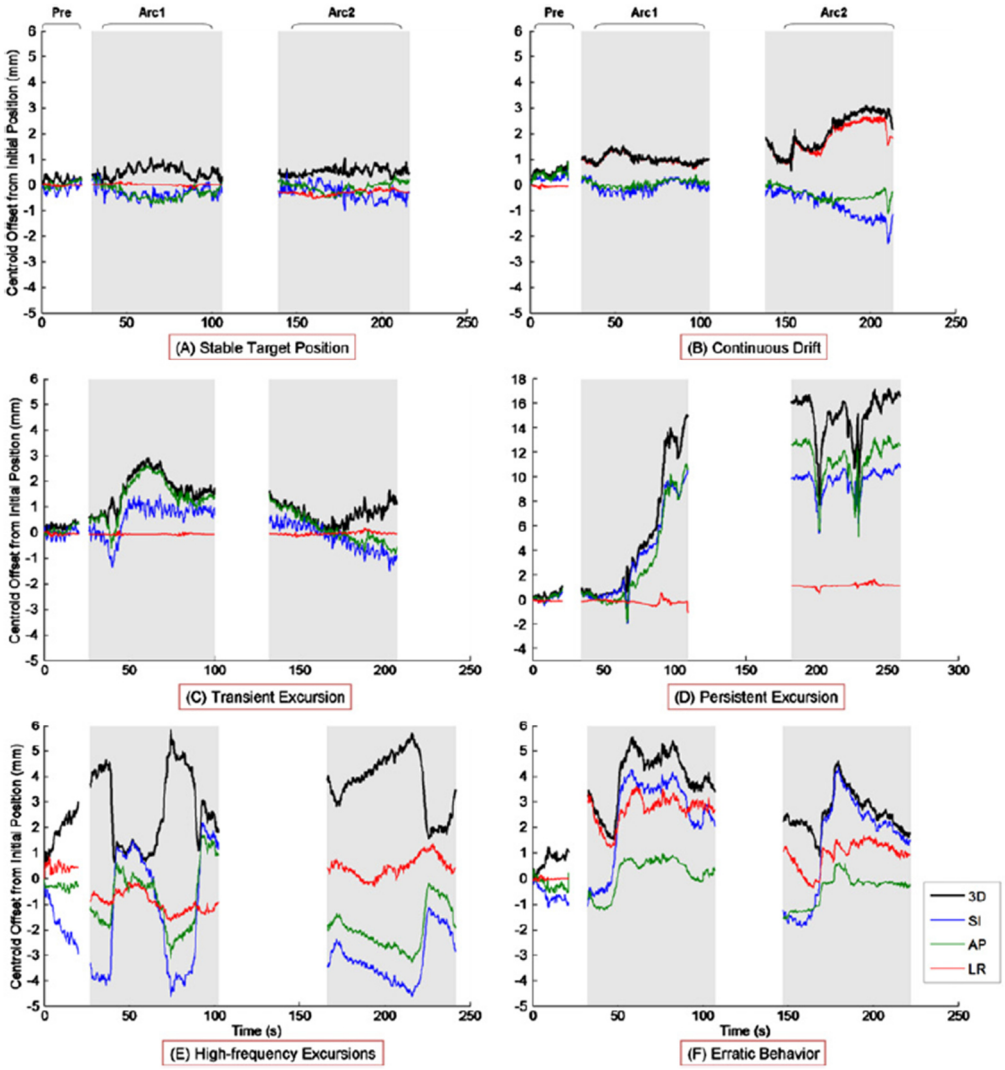

Figure 4. Trajectories of prostate motion during IMAT (2 arcs) reported by Ng et al (2012). The results are presented as control offset from initial position (mm) as a function of time (s). The motion was recorded using kilovoltage intrafraction monitoring (KIM) on implanted fiducial markers. Six different types of trajectories were identified; (A) stable target position, (B) continuous drift, (C) transient excursion, (D) persistent excursion, (E) high-frequency excursion and (F) erratic behaviour. The 3D (black), SI (blue), AP (green) and LR (red) trajectories are displayed. The grey intervals indicate beam-on.

Tong et al. (2015) monitored 200 patients, treated with intact prostates during a total of 7738 fractions, with the Calypso 4D localization system. The VMAT treatments were generally completed in five minutes and the majority of the patients did not exhibit any significant prostate motion during the course of a single fraction. However, in 59 fractions substantial prostate drifts larger than 5 mm were observed within the first minute after treatment setup. A drift larger than 3 mm was observed in 269 fractions. No typical patterns between these patients were identifiable, rather the drifts occurred randomly among the patients. Therefore, Tong et al suggest observations with real-time tracking systems of the patients for the first one or two weeks to identify the patients exhibiting severe intra-fractional motions.

Overall, prostate motion is generally small. The observed motions indicate little movement in the lateral direction (left-right, LR) (Ng et al., 2012, Both et al., 2011, Langen et al., 2008, Willoughby et al., 2006, Nederveen et al., 2002). Rather, the prostate is displaced in the anterior-posterior (AP) and superior-inferior (SI) directions. A study by Langen et al. (2008) also found that the AP-SI movement

was simultaneous, which was described as a likely consequence of bowel movements and muscular movement in the pelvic or lower extremities. Lin et al. (2013) observed a high correlation in AP-SI directional motions. They displayed the spatial distribution of the prostate motion, showing an elongated shape in oblique direction (AP-SI). Figure 5 is an example of the spatial distribution of the transponder displacement for three individual patients, including all fractions.

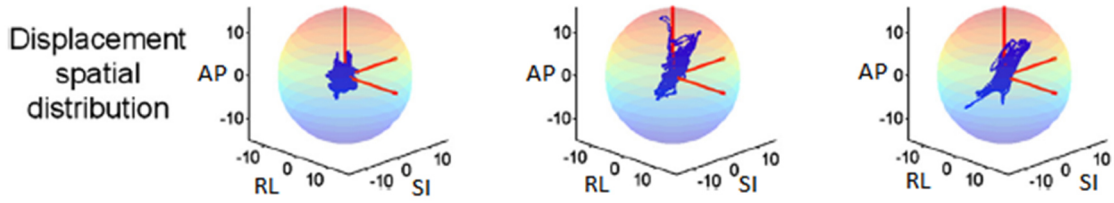

Figure 5. Extract of intra-fraction prostate motion monitored using Calypso 4D in a study by Lin et al (2013). The plots are examples of the spatial distribution of the implanted transponder displacement in three different patients, including all fractions. The motion is mainly in the AP and SI directions and is found to have a non-Gaussian distribution in most of the cases.

Even though the pattern of the prostate motion is complex and unpredictable, it seems that the displacement of the prostate increases with time. Ballhausen et al. (2015) monitored six patients over 84 fractions and a total of 9 hours and 25 minutes using 4D perineal ultrasound. In their article, they present the prostate motion as a random walk. They found that the position of the prostate relative to the isocenter continuously drifts over time during a fraction (Figure 6). Thus, treatment time should be kept as short as possible to minimise the drift. Several other studies have also found the prostate position to drift over time (Lovelock et al., 2015, Both et al., 2011, Langen et al., 2008). In fact, most available studies agree on the importance of keeping treatment times to a minimum (Tong et al., 2015, Lovelock et al., 2015, Ng et al., 2012, Shimizu et al., 2011, Shelton et al., 2011, Kupelian et al., 2007, Langen et al., 2008).

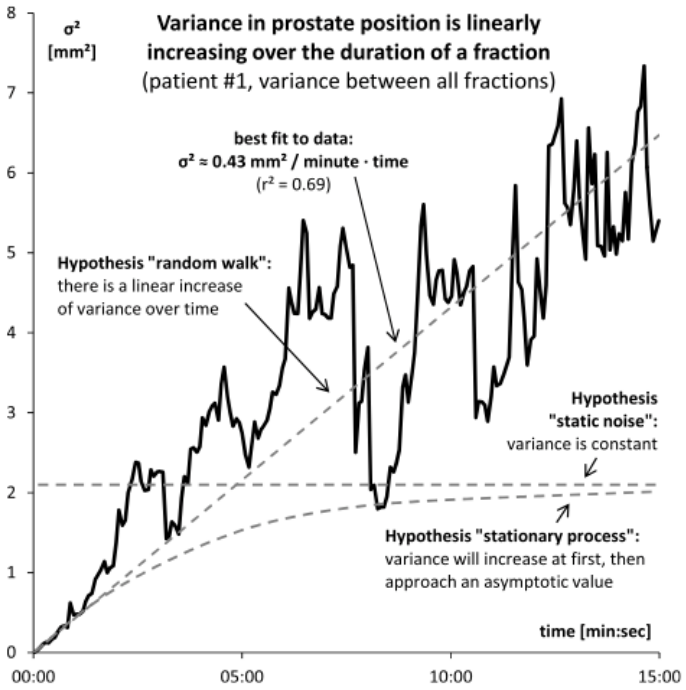

Figure 6. The variance in prostate position for one patient (22 fractions), showing good agreement with the linearly increasing variance predicted by the random walk model (Ballhausen et al., 2015).

Table 3.1. Overview of the publications included in this literature study of prostate motion.

Authours	Year	Patients (fractions)	Implants	Imaging modality	Imaging frequency
Tong, X et al	2015	236 (8660)	3 beacons	Calypso 4D localization system	10 Hz
Lovelock DM et al	2015	89	3 beacons	Calypso 4D localization system	10 Hz
Ballhausen H, et al	2015	6 (84)	-	4D ultrasound (Elekta Clarity system)	2 Hz
Huang CY et al	2015	10 (267)	3 gold fiducial markers	kV intra-fraction monitoring	5-10 Hz
Gladwish A et al	2014	30 (150)	3 gold fiducial markers	Pre- and post-treatment orthogonal images	160-388 s
Lin Y et al	2013	31 (1024)	3 beacons	Calypso 4D localization system	10 Hz
Cramer et al	2013	143 (4137)	Electromagnetic transponders	CBCT, electromagnetic transponder localization	10 Hz
Quon, H et al	2012	53 (265)	3 gold fiducial markers	Pre- and post-treatment orthogonal images	3-30 min
Ng, JA et al	2012	10 (268)	3 fiducial markers	kV intra-fraction monitoring	5-10 Hz
Mutanga TF et al	2011	21	4 gold markers	kV/MV orthogonal imaging	Simulation
Shelton J et al	2011	37 (1332)	3 beacons	Calypso 4D localization system	10 Hz
Shimizu S et al	2011	20 (4541)	3 fiducial markers	Fluoroscopy, real-time tracking	1-3 min
Poulsen PR et al	2009	17 (548)	Electromagnetic transponders	kV imaging (single)	0.5, 1, 2 and 5 Hz
Langen KM et al	2008	17 (550)	3 beacons	Calypso 4D localization system	10 Hz
Kupelian PA et al	2007	41	3 beacons	Calypso 4D localization system	10 Hz
Willoughby TR et al	2006	11	3 beacons	Calypso 4D localization system	10 Hz
Mah D et al	2002	42	-	Cine MRI	7-9 s
Nederveen et al	2002	10 (251)	3 gold markers	Si-flat panel imager	400 ms
Padhani AR et al	1999	55	-	Cine MRI	10 s

4 MATERIAL AND METHODS

4.1 TREATMENT PLANNING

4.1.1 PATIENT MATERIAL

The selection of the patient material was made from the database of the HYPO-RT-PC trial (Widmark et al., 2014). For the purpose of this study, nine patients, were chosen based on prostate size ("small", "medium" and "large") in order to investigate the treatment delivery for a range of clinical target volumes (CTV). The sizes were categorised based on the entire patient population (805 patients) registered so far in the HYPO-RT-PC study. The median CTV volume was 54 cm^3, with a lower quartile of 44 cm^3 and an upper quartile of 69 cm^3. The three patients who most recently received their treatment were selected from each group. They had all received VMAT in Lund between 2013-2015. Five patients were originally treated in the conventional arm (C), 78.0 Gy in 39 fractions, while four patients had been treated in the hypofractionated arm (H), 42.7 Gy in 7 fractions. Patient details are summarized in Table 4.1.

This study was approved by the Regional Ethics Board of Lund, Sweden (EPN Lund, Dnr 2013/742).

Table 4.1 Patient baseline characteristics.

Patient	Age [yrs]	Arm*	Prostate size	CTVvol [cm^3]	T-stage	PSA [µg/l]	Gleason score	GLS1 + GLS2
1	72	C	Small	35.1	2	3.3	7	4 + 3
2	61	H	Small	38.6	1c	4.0	7	3 + 4
3	73	C	Small	37.2	2	4.3	7	3 + 4
4	66	C	Medium	54.1	2	4.3	7	4 + 3
5	72	H	Medium	55.0	1c	4.9	7	4 + 3
6	71	H	Medium	52.0	1c	5.1	7	3 + 4
7	65	C	Large	82.5	1c	11.0	7	3 + 4
8	73	C	Large	79.9	2	9.4	7	3 + 4
9	70	H	Large	81.6	2	6.4	7	3 + 4

* Original treatment arm: Conventional arm (C), hypofractionated arm (H)

4.1.2 TREATMENT PLANS AND OPTIMIZATION

The original delineation of the clinical target volume (CTV), planning target volume (PTV) and the organs at risk (OAR) were kept. Eight patients had images from CT fused with MR images. One patient had CT images only. The outlining of the targets and OARs was done according to the trial protocol (Widmark et al., 2014). The CTV was defined as the prostate on the CT image set with MR guidance if available. The PTV accounts for uncertainties in delineation as well as internal movements and set-up. The PTV is defined as the CTV plus a 7 mm isotropic margin.

Three-dimensional treatment planning was done on the CT image set (3 mm slice thickness) using the Eclipse Treatment Planning System (TPS) version 13 (Varian Medical Systems). Absorbed dose calculations were performed on calculation grids of 2.5 mm, using the Analytical Anisotropic Algorithm (AAA) version 10.0.28. The beam qualities and the notation used when generating the VMAT plans were 10 MV flattened beam (10X), 6 MV unflattened beam (6FFF) and 10 MV unflattened beam (10FFF). The three plans were created for the conventional arm (C) and the hypofractionated arm (H) of the study, respectively. The same plan could not be used for both arms, as the optimization process was based on dose specific study protocols. In total, 54 treatment plans were generated (6 treatment plans for each patient).

At the radiotherapy department in Lund a beam quality of 10 MV with flattening filter is used for prostate cancer treatments. An example of the dose distribution in a hypofractionated standard beam

quality plan, H10X, is presented in Figure 7. All 10X plans were created according to the normal clinical routines at the department. As there is not yet a clinical routine for unflattened beams treating prostate cancer, these were created in a similar way to give equal or improved dose distribution, while fulfilling the defined dose constraints. One 360° arc was used to fulfil the dose constraints in each plan. The collimator angle was set to 5°. The maximum available dose rate was allowed for all beams; 600 MU/min for 10 MV flattened beams, 1400 MU/min for 6 MV unflattened beams and 2400 MU/min for 10 MV unflattened beams. Common plan properties are reported in Table 4.2.

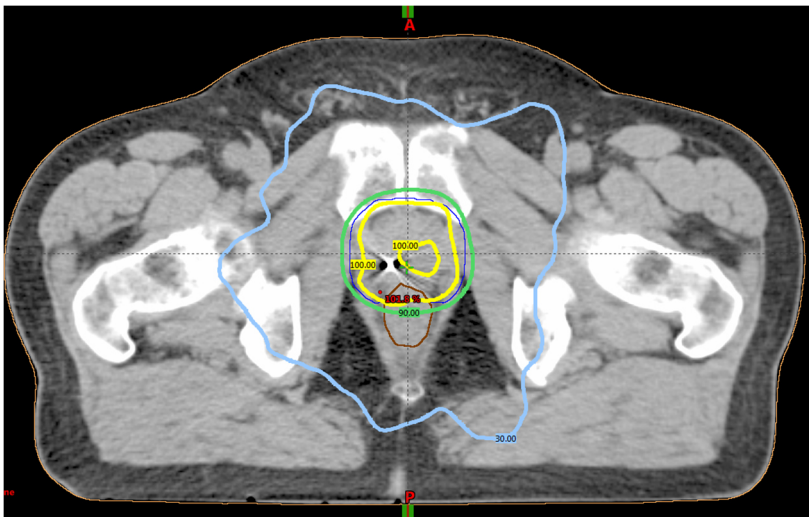

Figure 7. Example of the dose distribution, showing the isodose levels of 30% (light blue), 90% (green) and 100% (yellow) in the hypofractionated 10 MV flattened (H10X) treatment plan for patient 1.

Table 4.2. Common properties of the VMAT treatment plans created for each patient.

Plan	Study arm	Prescribed dose	Energy	Flattening filter	Collimator angle [°]	Arc	Max doserate [MU/min]
C10X	Conventional	2.0 Gy x 39	10 MV	Yes	5	1	600
H10X	Hypo	6.1 Gy x 7	10 MV	Yes	5	1	600
C6FFF	Conventional	2.0 Gy x 39	6 MV	No	5	1	1400
H6FFF	Hypo	6.1 Gy x 7	6 MV	No	5	1	1400
C10FFF	Conventional	2.0 Gy x 39	10 MV	No	5	1	2400
H10FFF	Hypo	6.1 Gy x 7	10 MV	No	5	1	2400

The dose constraints are specified in the HYPO-RT-PC study protocol version 6 and are reported in Table 4.3. The initial setting used for the VMAT optimization was start dose, end dose and fall-off for Normal Tissue Objectives (NTO) and upper and lower objectives on the PTV. When necessary, a lower objective of the prescribed dose was also introduced on the CTV. Upper objectives on the rectum were lowered interactively during optimization. Fixed upper objectives were used on the right and left femoral heads. The priorities on the OARs were all lower than for the NTO, the PTV and the CTV. Two optimizations were performed on every treatment plan. All plans were normalized to the PTV average dose in accordance with the trial protocol.

The objectives were optimized individually for each plan in order to fulfil the dose constraints as defined in the protocol. Other studies (Zwahlen et al., 2012, Gasic et al., 2014) report on using the same objectives on all plans for each patient. However, this would not suit the aim of this particular study since the purpose is to investigate the clinical relevance of the different beam qualities and not an evaluation of the treatment planning system itself.

The treatment plans were visually reviewed and approved by a senior clinical physician at the radiotherapy department.

Table 4.3. Dose-volume objectives to target volumes and organs at risk.

Priority	Volume	Conventional arm	Hypofractionated arm	Comment
1	CTV	$D_{min} \geq 95\%$ $D_{min} \geq 74$ Gy	$D_{min} \geq 95\%$ $D_{min} \geq 40.6$ Gy	The minimum dose to CTV shall be greater than or equal to 95% of the prescribed dose, i.e. $D_{mean,PTV}$
2	PTV	$V_{74Gy} \geq 95\%$ $V_{95\%} \geq 95\%$	$V_{40.6Gy} \geq 95\%$ $V_{95\%} \geq 95\%$	The 95% isodose shall cover at least 95% of PTV.
3	Rectum	$V_{70Gy} \leq 15\%$ $V_{90\%} \leq 15\%$	$V_{38.4Gy} \leq 15\%$ $V_{90\%} \leq 15\%$	Less than 15% of the outlined rectal volume should receive doses greater than 90% of the prescribed dose.
4	PTV	$D_{99\%} \geq 70$ Gy $D_{99\%} \geq 90\%$	$D_{99\%} \geq 38.4$ Gy $D_{99\%} \geq 90\%$	The "near minimum dose" to PTV should be greater than or equal to 90% of the prescribed dose.
5	Rectum	$V_{59Gy} \leq 35\%$ $V_{75\%} \leq 35\%$	$V_{32Gy} \leq 35\%$ $V_{75\%} \leq 35\%$	Less than 35% of the outlined rectal volume should receive doses greater than 75% of the prescribed dose.
6	Femoral heads	$D_{max} \leq 55$ Gy $D_{max} \leq 70\%$	$D_{max} \leq 29.9$ Gy $D_{max} \leq 70\%$	The maximum dose to the femoral heads should be less than or equal to 70% of the prescribed dose.
7	Rectum	$V_{51Gy} \leq 45\%$ $V_{65\%} \leq 45\%$	$V_{28Gy} \leq 45\%$ $V_{65\%} \leq 45\%$	Less than 45% of the outlined rectal volume should receive doses greater than 65% of the prescribed dose.
8	Body	$D_{max} \leq 82$ Gy $D_{max} \leq 105\%$	$D_{max} \leq 44.9$ Gy $D_{max} \leq 105\%$	The maximum global dose should be less than or equal to 105% of the prescribed dose.

The DVH parameters stated in the trial protocol (Table 4.3) were extracted from Eclipse. The mean and the standard deviation for the nine patients for each of the beam qualities and treatment arms were calculated. Combined DVHs were created (displaying PTV, CTV and rectum) using the mean of all patients for each plan category.

4.1.2.1 RECTUM PARAMETERS

In the treatment protocol it is stated that the anterior-posterior (AP) diameter of rectum should not exceed 40 mm at the level of the prostate position in the CT image set. However, the patients do not receive any guidelines on emptying rectum prior to the CT scan or the treatment sessions. The only recommendation is that the patient should have a "comfortably filled bladder" (Widmark et al., 2014).

The maximum AP rectum diameter in the cohort of patients selected for this study was measured in each of the CT image sets. The volumetric overlap in the structures of rectum and PTV was also calculated, using a Boolean operator in Eclipse.

4.1.3 VERIFICATION TREATMENT PLANS

The treatment plans were recalculated, creating verification plans where the patient's CT data set was replaced by the Delta^4 phantom (Figure 8). The verification plan was imported to the Delta^4 software, allowing for a comparison between the measured and the calculated doses. This patient QA was performed for all VMAT patients.

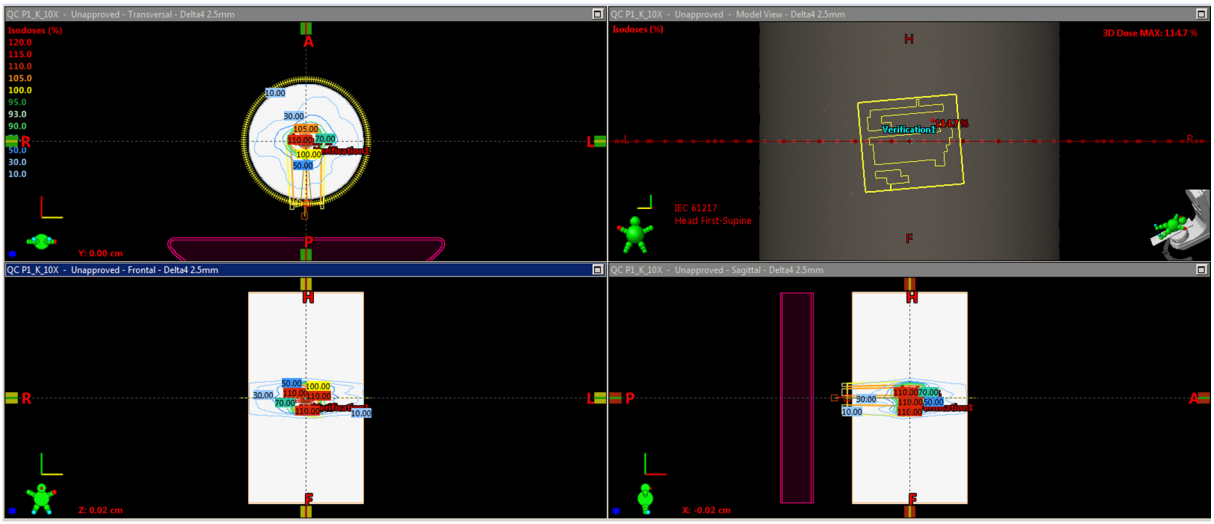

Figure 8. An example of the dose distribution in the verification plan of conventional flattened 10 MV (C10X) for one of the patients. The dose distribution is displayed in the transversal (upper left), coronal (lower left) and sagittal (lower right) planes. The upper right image shows the starting position of the MLC in beams eye view.

4.2 TREATMENT DELIVERY

The medical linac used for measurements in this study was a Varian TrueBeam™. The output of the linac was checked by performing the department's monthly dose output verification procedure before the measurements were run. The tolerance on dose deviations for these tests is set to 1%. The low tolerance ensures that large drifts in dose output are prevented. Gantry and collimator angles were set to 0°. The ion chamber (PTW 30012) was placed inside a polystyrene block attached to the gantry. Temperature and pressure were measured. A field size of 15x15 cm^2 was set using the collimator jaws; the multi leaf collimator (MLC) was completely withdrawn. The ion chamber was pre-irradiated with 500 MU. Three measurements of 100 MU for each of the beam qualities 10 MV, 6 MV FFF and 10 MV FFF were recorded. The reading of the electrometer was corrected for pressure and temperature and compared to a reference value. For all beam qualities, dose deviations were approximately 0.5%, which is below the tolerance for monthly controls. Basic output and dose profile controls are performed on a daily basis using a 2D quality assurance device.

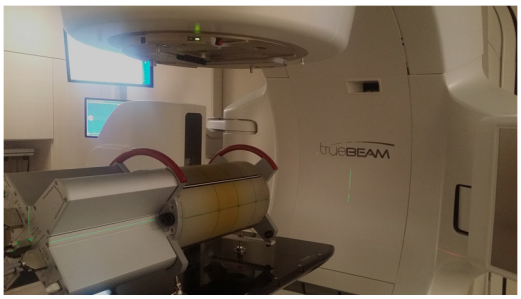

Figure 9. The Delta^4 phantom setup.

To ensure the quality of the dose measurements, the Delta^4 dosimetry system is calibrated at installation and thereafter as appropriate. Before the treatment plans of this study were measured a full calibration was carried out. The phantom was irradiated using a 10x10 cm^2 open field for all beam qualities. A cross-calibration was performed for the two Delta^4 detector planes. A relative calibration

was performed for one photon energy (with flattening filter) in order to determine the sensitivity of every individual detector. For the absolute calibration all available photon energies were evaluated, both flattened and unflattened beams. Finally a directional calibration was made to determine variations due to rotational direction-dependence. The detector planes were irradiated upside down and the measurements were compared to the ones with normal beam incidence to identify any deviations.

After the calibration, the Delta^4 phantom was carefully positioned isocentrically using the set-up lasers (Figure 9). The phantom was connected to the accelerator, sending a trigger pulse to the phantom to start the measurement collection. Each of the patient specific treatment plans were delivered to the phantom, whereby the collected data was organized based on gantry angle. The planned dose distribution was imported from the TPS. In this work the planned dose for each control point was compared to the corresponding measured dose by the diodes of the two orthogonal detector planes using gamma evaluation.

Treatment times were recorded manually on a stopwatch and in the verification system (Aria).

4.3 MOTION STUDY

A study on the effects of prostatic displacement during treatment delivery was also designed. For this purpose the patient with the longest treatment times was selected. The treatment plans H10X and H10FFF were used to evaluate the impact of intrafractional prostate motion. To simulate motion the Delta^4 was connected to the Hexamotion module (ScandiDos, Uppsala, Sweden). Trajectory data were received from Ng et al. (2012), University of Sydney, Australia. The patterns are shown in Figure 4.

A trajectory convertor was constructed in MATLAB to adapt the data to the format used as input files to the Hexamotion. The time resolution and movements that were too rapid or had too steep gradients to be accepted by the Hexamotion were slightly adjusted, keeping the characteristics of the trajectory.

The selected treatment plans were delivered for six different motion patterns (stable trajectory, continuous drift, persistent excursion, transient excursion, high-frequency excursions and erratic behaviour). The plans were also delivered in a static reference situation with the Delta^4 positioned in the defined origin. The treatment delivery (beam-on) was started at the same time as the trajectory (Hexamotion), for all but two trajectories. These two were cropped in order to be able to study the effects. Delivery with transient excursion was started 60 s into the motion pattern for both plans. This time interval may represent the time it takes to review the daily set-up images, before the treatment. The delivery with transient excursion was started at 175 s for H10X and at 200 s for H10FFF to include the peak in the trajectory and investigate the effect of the temporal displacement.

All results were evaluated relative to the static delivery.

4.4 EVALUATION OF MEASUREMENTS

4.4.1 PLAN EVALUATION

The delivered dose distribution of the treatment plans was measured with the Delta^4 pre-treatment verification phantom. The results obtained in the ScandiDos software are based on dose deviation, distance-to-agreement and gamma indices (section 3.6). Histograms from the three evaluation methods are presented in the software evaluation dialog as well as dose profiles showing the calculated and the measured doses.

The homogeneity index (HI) and the conformity index (CI) were calculated and used as a further comparison of the plan quality. Variables included in the calculation were extracted from the respective DVH. The homogeneity index was calculated, as defined in ICRU 83, from the following expression

$$HI = \frac{D_{2\%} - D_{98\%}}{D_{50\%}} \quad \textbf{(13)}$$

where $D_{2\%}$ is the near-maximum absorbed dose, $D_{98\%}$ is the near-minimum dose and $D_{50\%}$ is the median dose.

The conformity index, as defined by Paddick (2000), was calculated from

$$CI = \frac{TV_{PIV}^2}{TV \cdot PIV} \quad \textbf{(14)}$$

where TV is the target volume (PTV), PIV is the volume within the prescribed isodose ($V_{95\%}$ for the structure BODY) and TV_{PIV} is the volume of the PTV surrounded by the prescribed isodose ($V_{95\%}$ for the PTV).

The evaluation of the treatment delivery was done using gamma indices with different passing criteria (3% and 2mm, 2% and 2mm, 2% and 1mm and 1% and 1mm, respectively). The calculated dose distribution is compared to the measured dose, collected by each diode of the two orthogonal detector planes. In the department in Lund a pass rate of 90 % is required for the gamma criteria 3% and 2 mm for all clinical treatment plans. However, if the pass rate is below 95 % the plan is further analysed to evaluate the clinical relevance of any deviations. Additionally, the dose distribution profile to profile and point to point is also reviewed for the individual treatment plans.

4.4.2 STATISTICAL ANALYSIS

Before any statistical tests were run, the results were checked for normality using the Kolmogorov-Smirnov test.

A two-tailed paired sampled student's t-test was used to evaluate if any differences between the flattened and unflattened beams were significant. The level of significance was set to 5 %. Correlation between the different parameters was investigated using Pearson's correlation coefficient and linear regression.

5 RESULTS

The results presented below are based on six subgroups of treatment plans, using beam qualities of 10 MV, 6 MV FFF and 10 MV FFF for both conventional and hypofractionation schedules, created for nine different patients (54 treatment plans in total).

5.1 TREATMENT PLAN QUALITY: DOSE DISTRIBUTION

The fundamental parameters of interest in this study were beam quality and treatment technique. Hence, all treatment plans were evaluated on dose-volume constraints (based on the protocol described in Table 4.3), homogeneity and conformity index, plan complexity (expressed as MU/Gy) and visual appearance of the homogeneity/inhomogeneity in dose distribution.

The treatment plans were reviewed by a senior physician in the radiotherapy department, who approved all plans to be clinically acceptable. The dose coverage of the target was met in all beam qualities. A thorough analysis of the plans was carried out on each of the cumulative dose-volume histograms (DVH). The dose constraints, specified in the HYPO-RT-PC protocol (Table 4.3), were compared to the corresponding value derived from the DVH. The average cumulative DVH for all patiens, computed for the six subgroups, are presented in Figure 10. The main prioritised structures are included in the DVH; CTV, PTV and rectum.

All objectives were met by all patients. Comparing the mean of all nine patients, no significant differences were found between the different beam qualities or between the different fractionation schedules. A detailed summary of the mean values from all patiens (with one standard deviation uncertainty) for all protocol parameters can be found in Table 5.1.

The dose bath was calculated for all beam qualities, using $V_{10\%}$ and $V_{5\%}$ for the total CT volume. No significant differences were found for the mean of the nine patients between flattened and unflattened beams. The volumes were slightly smaller, but not significant, for 10FFF than for both 10X and 6FFF in the conventional and hypofractionated plans. These results were based on the calculations from the treatment planning system. Further measurements in the low dose area would be required for a more accurate evaluation of the dose bath.

The homogeneity and the conformity indices of the PTV were calculated using equations 13 and 14, respectively (Table 5.1). The results of the three beam qualities in both experimental arms were all within one standard deviation relative to eachother. Hence, there was no statistical significance in target coverage between flattened and unflattened beams.

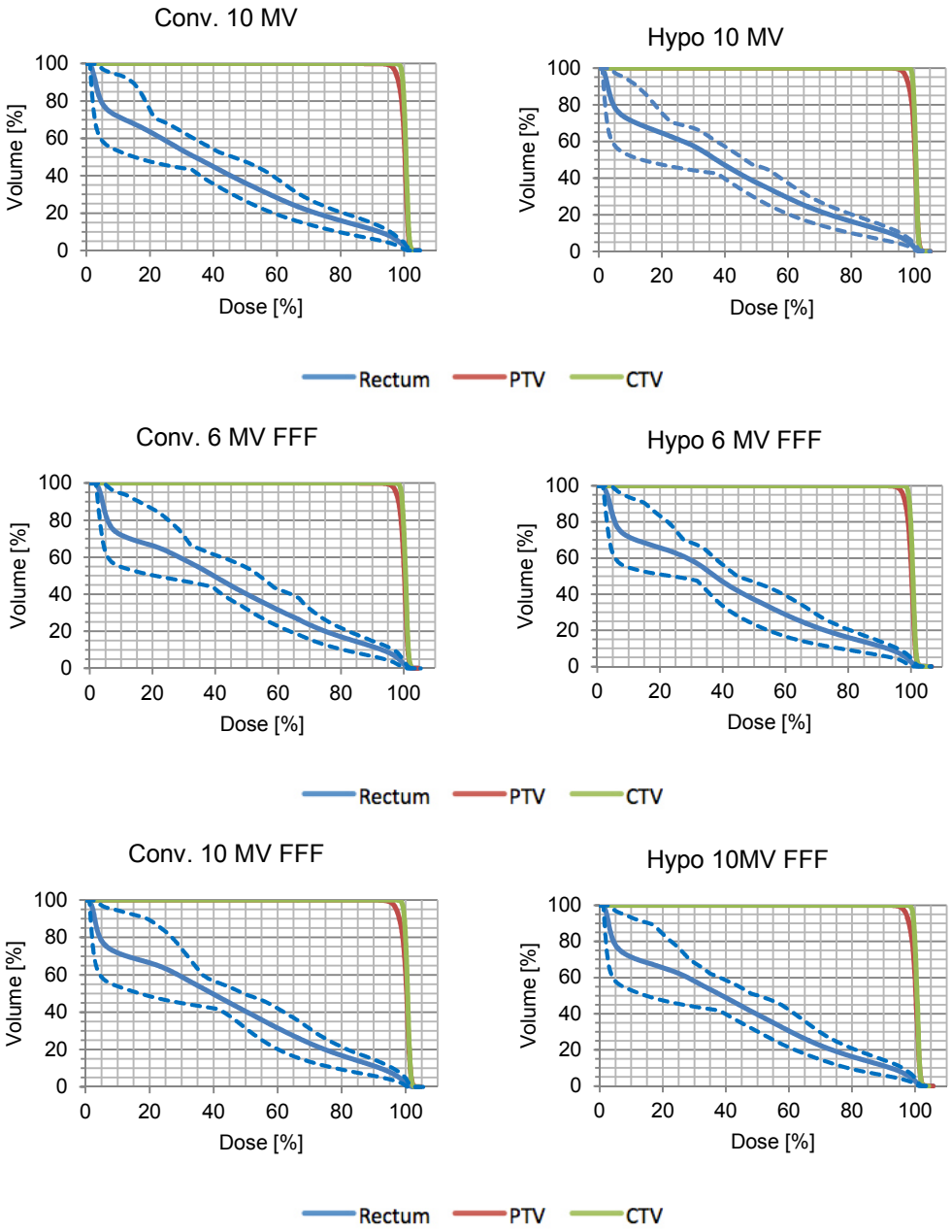

Figure 10. The cumulative mean dose volume histograms (DVH) computed for all patients for each of the treatment plans. The red and green solid lines represent the mean cumulative dose to PTV and CTV, respectively. The blue solid line represents the mean cumulative dose to rectum and the blue dashed lines illustrate the range of mean rectum dose in the patient cohort.

Table 5.1 DVH parameters (mean values ±1SD), based on all patients. Upper table displays the results for the conventional plans and lower table displays the hypofractionated plans.

	Objective	C10X	SD	C10FFF	SD	C6FFF	SD
CTV Mean	**[Gy]**	78.37	± 0.07	78.46	± 0.11	78.40	± 0.09
CTV Min	**≥ 74 Gy**	76.13	± 0.67	76.08	± 0.53	75.86	± 0.44
PTV $V_{95\%}$	**≥ 95%**	99.44	± 0.35	99.09	± 0.73	99.49	± 0.43
Rectum $V_{90\%}$	**≤ 15%**	11.22	± 2.90	11.29	± 2.94	11.79	± 2.91
PTV $D_{99\%}$	**≥ 70 Gy**	74.60	± 0.44	74.22	± 0.69	74.74	± 0.57
Rectum $V_{75\%}$	**≤ 35%**	18.52	± 4.21	19.87	± 4.70	20.01	± 4.73
FH dx Max	**≤ 55 Gy**	30.59	± 5.22	30.26	± 3.44	30.20	± 6.41
FH sin Max	**≤ 55 Gy**	33.47	± 5.39	31.87	± 4.40	31.85	± 5.11
Rectum $V_{65\%}$	**≤ 45%**	24.52	± 5.32	27.31	± 6.40	27.61	± 7.01
Body Max	**≤ 82 Gy**	81.01	± 0.34	81.40	± 0.50	81.64	± 0.86
Body Mean	**[Gy]**	3.85	± 0.58	3.75	± 0.51	4.13	± 0.59
Body $V_{10\%}$	**[%]**	14.40	± 1.99	13.89	± 1.79	14.47	± 1.98
Body $V_{5\%}$	**[%]**	17.57	± 2.10	17.10	± 1.91	17.69	± 1.99
CI	**1**	0.889	± 0.016	0.894	± 0.015	0.871	± 0.021
HI	**0**	0.054	± 0.006	0.061	± 0.009	0.053	± 0.007

	Objective	H10X	SD	H10FFF	SD	H6FFF	SD
CTV Mean	**[Gy]**	42.90	± 0.04	42.94	± 0.06	42.94	± 0.05
CTV Min	**≥ 40.6 Gy**	41.82	± 0.24	41.55	± 0.40	41.54	± 0.26
PTV $V_{95\%}$	**≥ 95%**	99.43	± 0.43	99.26	± 0.49	99.46	± 0.59
Rectum $V_{90\%}$	**≤ 15%**	11.31	± 2.71	11.21	± 2.91	11.28	± 2.80
PTV $D_{99\%}$	**≥ 38.4 Gy**	40.83	± 0.28	40.73	± 0.28	40.88	± 0.37
Rectum $V_{75\%}$	**≤ 35%**	18.98	± 3.80	19.11	± 3.80	18.65	± 4.26
FH dx Max	**≤ 29.9 Gy**	16.96	± 3.91	17.36	± 3.06	16.81	± 3.48
FH sin Max	**≤ 29.9 Gy**	17.53	± 2.71	17.54	± 3.24	17.82	± 2.58
Rectum $V_{65\%}$	**≤ 45%**	25.25	± 4.64	26.21	± 5.41	24.98	± 5.77
Body Max	**≤ 45.7 Gy**	44.38	± 0.27	44.61	± 0.32	44.74	± 0.51
Body Mean	**[Gy]**	2.08	± 0.31	2.07	± 0.30	2.27	± 0.32
Body $V_{10\%}$	**[%]**	14.27	± 2.00	14.07	± 1.97	14.65	± 1.93
Body $V_{5\%}$	**[%]**	17.49	± 2.06	17.13	± 2.02	17.77	± 2.01
CI	**1**	0.891	± 0.013	0.891	± 0.013	0.877	± 0.017
HI	**0**	0.055	± 0.007	0.059	± 0.007	0.055	± 0.010

The number of monitor units (MU) per dose unit (Gy), here defining the complexity of the treatment plans, are presented in the boxplot in Figure 11. Out of all the data, two values were considered outliers (deviated more than ±2.7σ), one value in the group C10X and one in H6FFF, plotted individually as red crosses. All sets of data were found to be normally distributed. An ANOVA test was performed on the variance between the six groups. The variance between the groups was found to be larger than that within the groups. The p-value, p=4e-08, implies that there is a significant difference in complexity of the plans between the groups.

The differences between the groups of beam qualities and fractionation schedules were statistically evaluated using a two-tailed paired sample student's t-test. The number of MU/Gy was significantly larger for all FFF plans ($p<0.05$) except for the conventional 10FFF plans ($p=0.19$). No significant difference was found comparing each of the beam qualities pairwise between the conventional and the hypofractionated plans. The 6FFF plans required the largest number of MU/Gy ($p<0.05$).

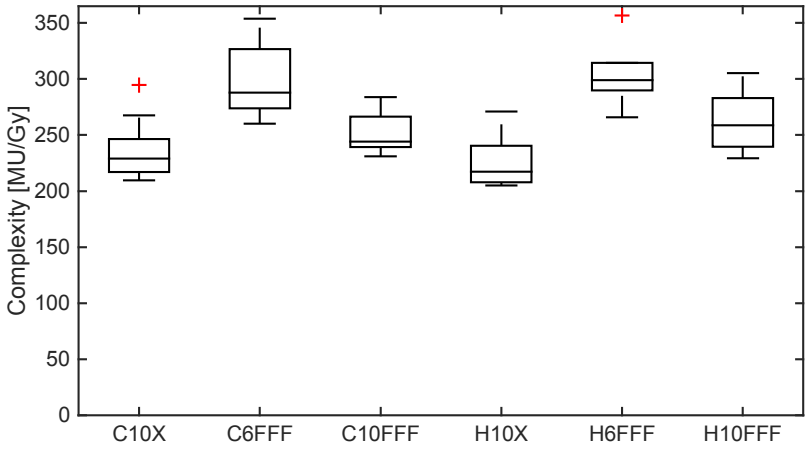

Figure 11. The complexity of the treatment plans for all patients, expressed in monitor units (MU) per prescribed dose (Gy). The line inside each box indicates the median, the box itself represents the 25th and 75th percentiles and the error bars are the range of values, excluding outliers. The outliers in the data are shown as red crosses (values deviating more than ±2.7σ).

A new anatomical structure was introduced, defined as the overlapping volume of rectum and PTV. For all patients, the volume of this structure was calculated. The defined volume is one of the conflicting areas in the dose optimization; the lower dose constraints on the PTV versus the upper dose constraints on rectum. The complexity (MU/Gy) was thus plotted as a function of the size of the overlapping volume. The results are presented in Figure 12. Moderate positive correlations (R^2 = 0.44 to 0.82) are observed for all groups of beam qualities, i.e. a larger overlapping volume requires a more complex plan in order to fulfil the dose constraints.

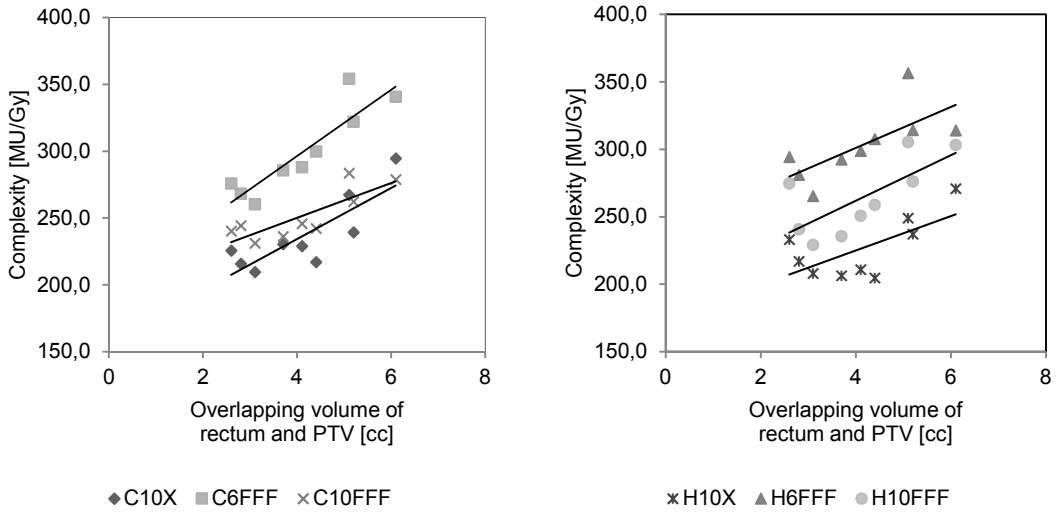

Figure 12. Complexity for the conventional (left) and the hypofractionated (right) treatment plans plotted as a function of volume overlap between rectum and PTV. A linear fit is applied to each of the subgroups of different beam qualities.

5.2 TREATMENT PLAN QUALITY: DELIVERY

5.2.1 TREATMENT TIME

The beam-on time for each plan delivery was measured. The results are presented in Figure 13. In the original treatment plans from the HYPO-RT-PC study (5 conventional, 4 hypo), the mean treatment times were 1.0 minute for C10X and 2.1 minutes for H10X. These are close to the times measured in this study. The conventional treatment plans were all delivered in 1.0 minute, with the exception of one C10X plan delivered in 1.1 minutes. The H10X plans had a mean delivery of 2.3 minutes (range: 2.1-2.8 minutes). For the unflattened beams the treatment times were significantly shorter; H6FFF plans were delivered in 1.3 minutes (range: 1.2-1.6 minutes) and the H10FFF plans were delivered in 1.0 minute (range: 1.00-1.04 minutes).

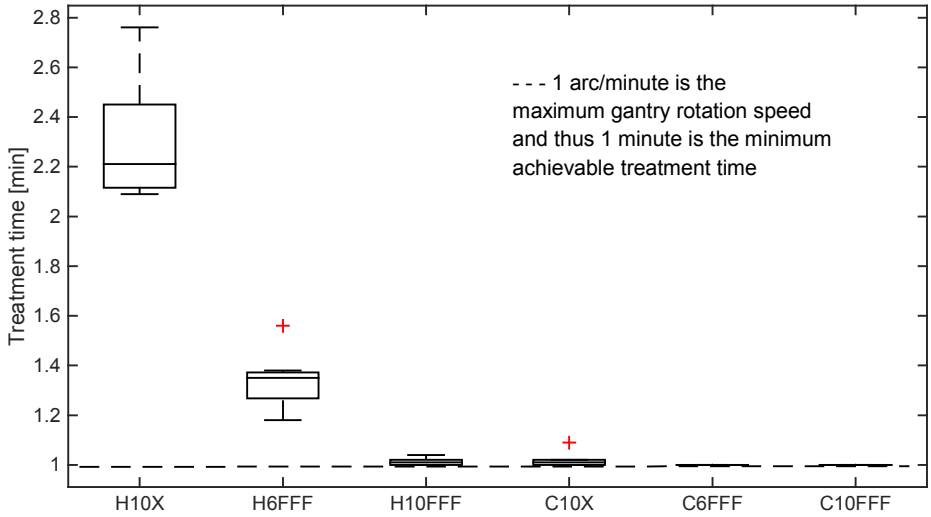

Figure 13. Beam-on time delivering single-arc treatments for all plans and beam qualities. Error bars indicate the range of recorded treatment times based on all patients in each subgroup of plans. The line inside each box is the mean treatment time. The outliers of the data are shown as red crosses (values deviating more than ±2.7σ).

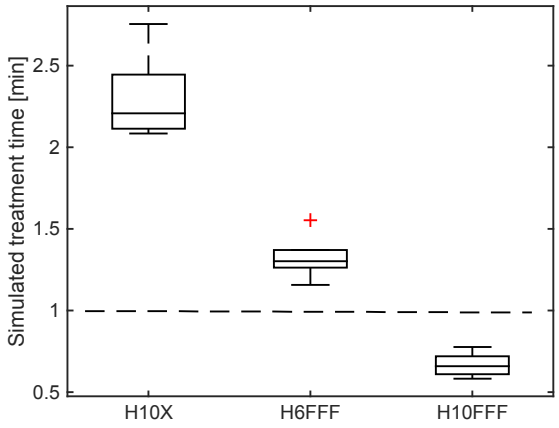

Figure 14. Theoretical treatment times of the hypo-fractionated plans, calculated from the number of MU per dose rate. The dashed line represents the actual minimum treatment time (1 min) due to restrictions on gantry rotation.

If the treatment time is simulated without accounting for the limited speed of the gantry, a further reduction in delivery time is observed for H10FFF (Figure 14). The 6.1 Gy per fraction could theoretically be delivered in less than one minute.

5.2.2 TREATMENT DELIVERY

The quality of treatment delivery for each of the created treatment plans was evaluated using measurements from the Delta[4] dosimetry phantom. The results were evaluated in the ScandiDos software using gamma indices with different criteria (from 3%, 2 mm to 1%, 1 mm). The pass rates for the treatment plans, divided into subgroup based on prostate size ("small", "medium" and "large") are presented as a function of complexity.

The results of the plans evaluated with the clinical acceptance gamma criteria used at the department in Lund (3%, 2 mm) are presented in Figure 15. The results of the pass rate for the 2%, 2 mm, the 2%, 1 mm and the 1%, 1 mm are presented in Figure 16, Figure 17 and Figure 18, respectively.

The subplots of Figure 15-18 each contain nine data points; the three patients with the defined prostate size ("small", "medium" or "large") and for every patient, the three corresponding treatment plans (conventional (left) or hypo (right)). The pass rate observed for the gamma criteria 3%, 2 mm (Figure 15) was well above the critical value of 90%, the lowest pass rate being 98.8%. Most plans had 100% of the points passing. No correlation was found between pass rate and prostate size or between pass rate and complexity. Furthermore, there was no significant difference in pass rate between the different beam qualities.

The pass rate decreased with increasing the stringencies of the gamma criteria. Similarly to the results of the 3%, 2 mm pass rate, no correlations were found between pass rate and prostate size, complexity or beam quality. All plans appeared to be delivered equally well.

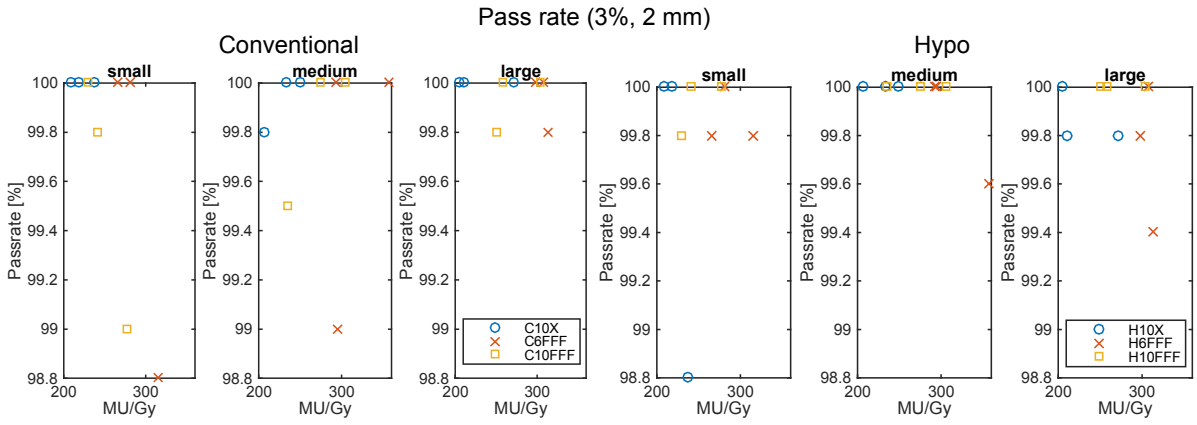

Figure 15. Results of measurements for all nine patients and all six treatment plans using gamma criteria 3 %, 2 mm. The reference value is the calculated dose.

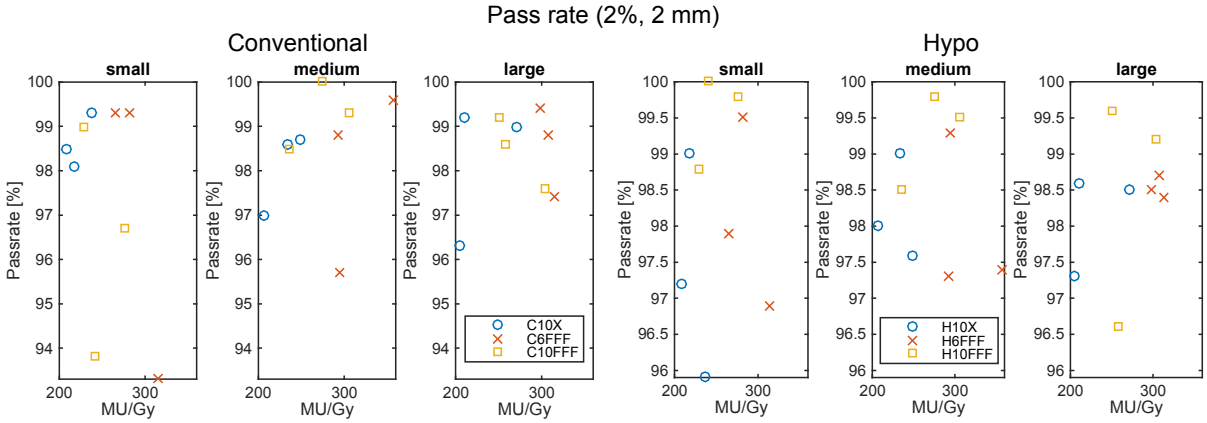

Figure 16. Results of measurements for all nine patients and all six treatment plans using gamma criteria 2 %, 2 mm. The reference value is the calculated dose.

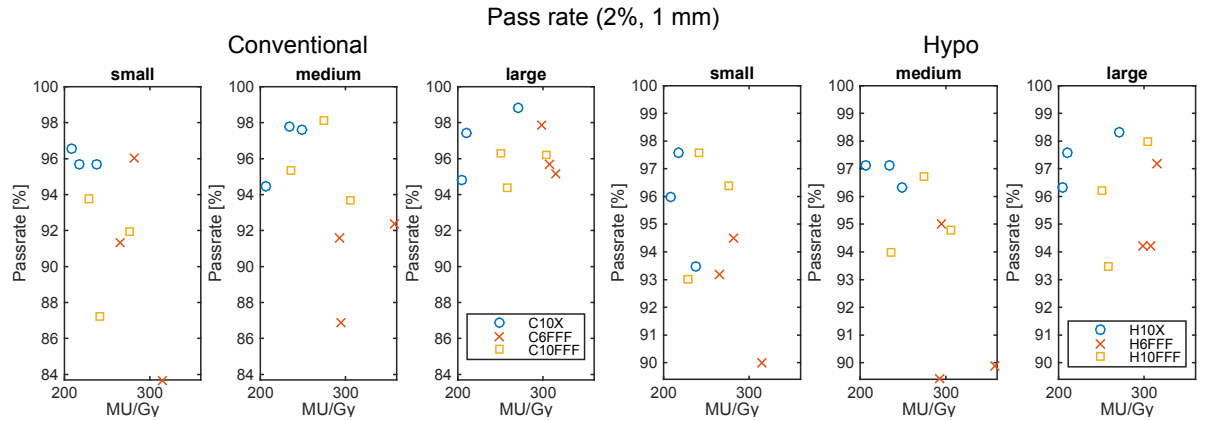

Figure 17. Results of measurements for all nine patients and all six treatment plans using gamma criteria 2 %, 1 mm. The reference value is the calculated dose.

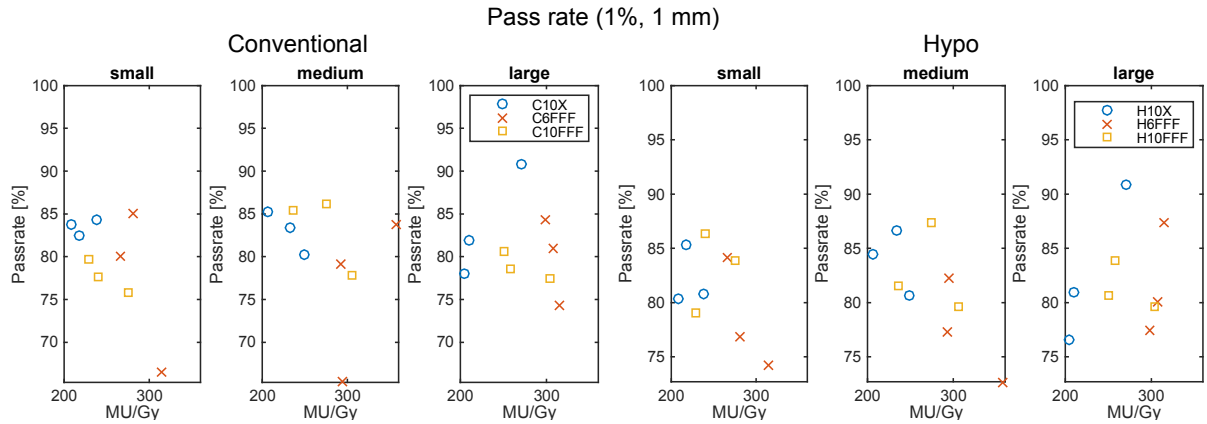

Figure 18. Results of measurements for all nine patients and all six treatment plans using gamma criteria 1 %, 1 mm. The reference value is the calculated dose.

5.3 MOTION STUDY

A motion study on the impact of prostate displacement was carried out using six different motion trajectories. The trajectory data was recorded by Ng et al (2012) and represent six typically observed prostate motion patterns. Each trajectory below was simulated for one patient during one fraction. The results were evaluated with a static treatment delivery as reference for the plans H10X and H10FFF. Below are the results from the evaluation of the mean dose using the same gamma criteria as above. Each trajectory is presented together with it's corresponding results. Note that the range of the y-axis, showing the prostatic displacement, varies between different trajectories.

The prostatic displacement of the "stable trajectory" (ST), Figure 19, and the "continuous drift" (CD), Figure 20, does not exceed more than 1 mm displacement in any direciton within the time frame of the two plan deliveries. The pass rate fraction relative the static delivery is 100% for all gamma criteria investigated, except for the H10X plan at 1% 1mm, which is just below. The treatements with the ST and the CD are delivered equally well, despite small offsets in position, for both the flattened and the unflattened beam.

The trajectory of "persistent excursion" (PE), Figure 21, was run for 60 s before the treatment was initiated. The effects on the pass rate of the H10X, delivered in 2.5 minutes, are more severe than on the H10FFF, delivered in 1.0 minute. Only for gamma criterion 1% 1mm is the pass rate for H10FFF less than for the static delivery.

The effect due the "transient excursion" (TE), Figure 22, was investigated by initiating the treatment such that it included the peak in offset in the respective time frame. The H10X plan was started 175 s into the trajectory, while the H10FFF plan was started after 200 s. The decrease in number of points passing the gamma criterion increases with stricter criteria for both treatment plans. The reduction in pass rate is somewhat greater for the H10FFF plan than for the H10X.

The effect observed in the results for the "high-frequency excursions" (HE), Figure 23, is similar to what is also observed for the "erratic behaviour" (EB), Figure 24. The pass rate decreases with stringency in gamma criteria for both treatment plans compared to the static delivery, where the largest decrease is observed for the H10X. When the gamma criterion is set to 1% 1mm, half as many points pass for the HE and the EB compared to the static case.

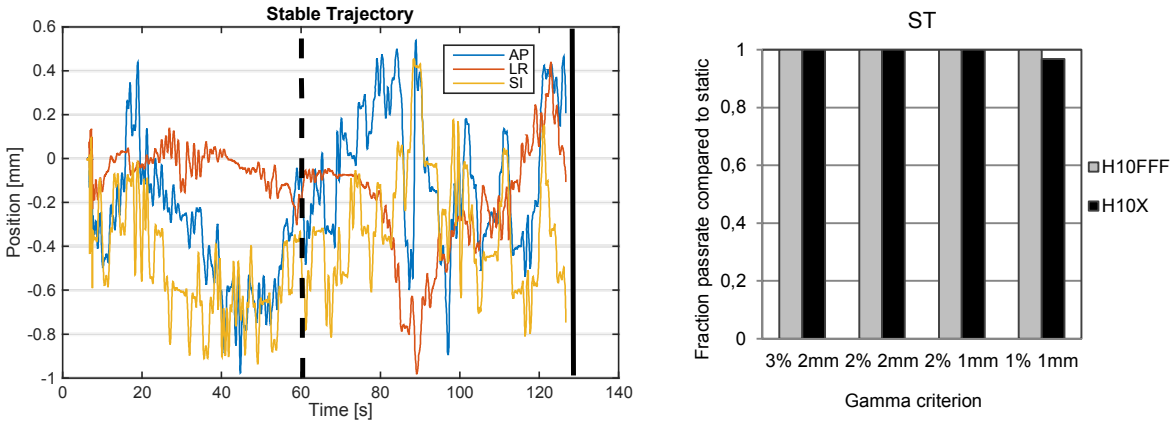

Figure 19. The stable trajectory (ST) is presented in three dimensions (left). The dashed and the solid black lines represent the end of the H10FFF treatment and the H10X treatment, respectively. The corresponding results of the gamma evaluation (right) relative to a static delivery are presented for H10FFF (grey) and H10X (black).

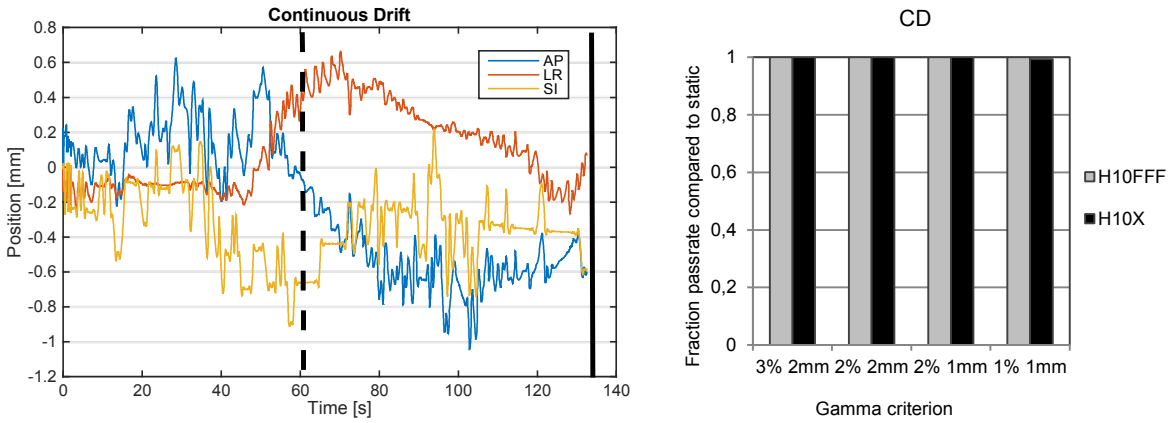

Figure 20. The trajectory of continuous drift (CD) is presented in three dimensions (left). The dashed and the solid black lines represent the end of the H10FFF treatment and the H10X treatment, respectively. The corresponding results of the gamma evaluation (right) relative to a static delivery are presented for H10FFF (grey) and H10X (black).

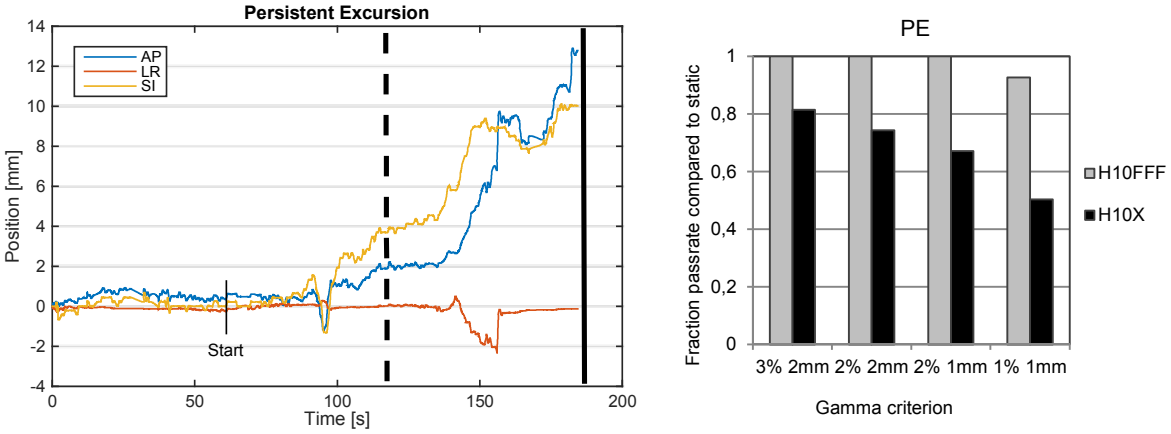

Figure 21. The trajectory of persistent excursion (PE) is presented in three dimensions (left). The dashed and the solid black lines represent the end of the H10FFF treatment and the H10X treatment, respectively. The corresponding results of the gamma evaluation (right) relative to a static delivery are presented for H10FFF (grey) and H10X (black). The treatment delivery was started at time = 60 s.

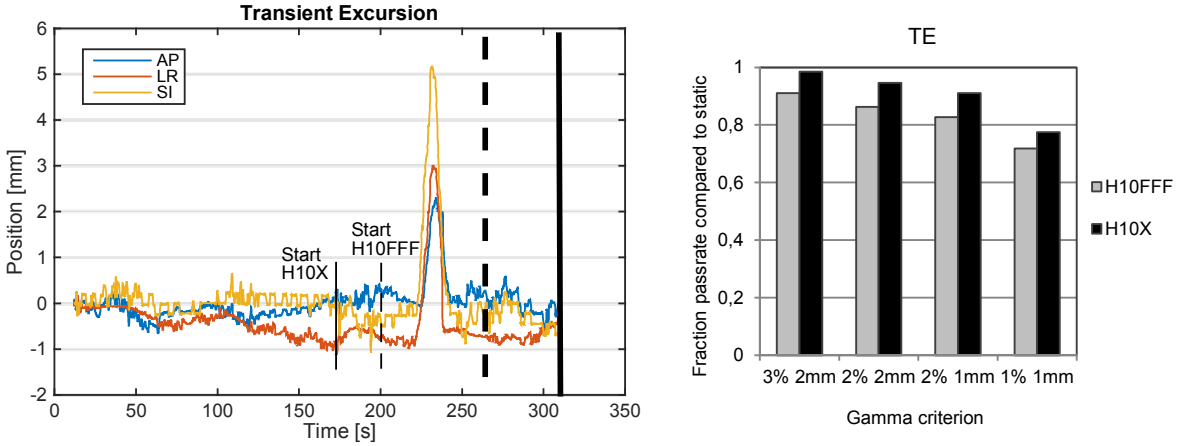

Figure 22. The trajectory of transient excursion (TE) is presented in three dimensions (left). The dashed and the solid black lines represent the end of the H10FFF treatment and the H10X treatment, respectively. The corresponding results of the gamma evaluation (right) relative to a static delivery are presented for H10FFF (grey) and H10X (black). The treatment delivery was started at time = 175 s for H10X and at time = 200 s for H10FFF.

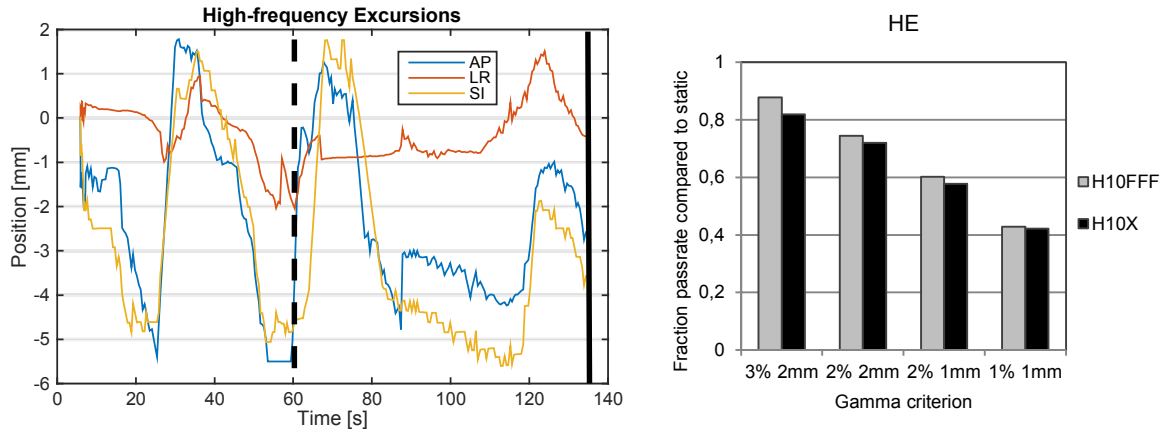

Figure 23. The trajectory of high-frequency excursions (HE) is presented in three dimensions (left). The dashed and the solid black lines represent the end of the H10FFF treatment and the H10X treatment, respectively. The corresponding results of the gamma evaluation (right) relative to a static delivery are presented for H10FFF (grey) and H10X (black).

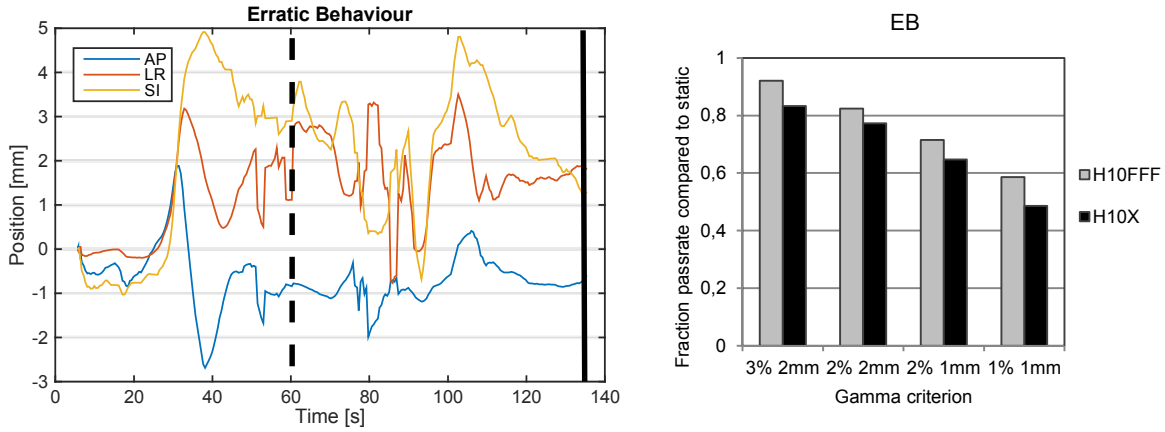

Figure 24. The trajectory of erratic behaviour (EB) is presented in three dimensions (left). The dashed and the solid black lines represent the end of the H10FFF treatment and the H10X treatment, respectively. The corresponding results of the gamma evaluation (right) relative to a static delivery are presented for H10FFF (grey) and H10X (black).

6 DISCUSSION

6.1 TREATMENT PLAN QUALITY: DOSE DISTRIBUTION

The results of this treatment planning study comparing plans for prostate cancer, performed using beams with and without flattening filter, show that the plans are generally of equal quality. None of the parameters extracted from the dose-volume histograms (DVH) differed significantly when comparing treatment plans with and without flattening filter. Part of the aim of this study was to investigate if the FFF plans could be generated with the same or improved quality as the standard plans. No improvement in treatment plan quality was observed, but the aim is nevertheless fulfilled, with similar dosimetric results for both flattened and unflattened beams.

The patients in the study were divided into three groups based on the volume of the prostate; "small", "medium" and "large". The mean of the large PTVs was more than double the volume of the small PTVs. Despite the large variation in target size, no compromise in plan quality was observed between the beam qualities. The plans were also robust to patient weight. For a larger patient a possible benefit might be expected from the FFF beams, since there is less variation in dose characteristics with depth for an unflattened beam. However, no such effect was observed in this cohort of patients.

All dose-volume objectives for all patients and all plans were within the constraints of the HYPO-RT-PC study protocol. Hence, all treatment plans would be acceptable for clinical use. The manual work during the optimization process of the treatment plans was similar irrespective of what beam quality was chosen. Planning the prostate cases with FFF beams instead of standard beams would therefore not imply any additional workload on the dose planning staff.

Although a higher integral dose to healthy tissue associated with unflattened beams has been of concern (Vassiliev et al., 2009), no significant difference between the beam qualities in integral dose, $V_{10\%}$ or $V_{5\%}$, was observed in this study. The dose bath as well as the integral dose was actually lower for the 10 MV FFF plans than for plans of the same energy with flattening filter. The corresponding doses for 6 MV FFF were marginally higher, which is in agreement with dose characteristics of lower energies and therefore expected. Either way, none of these differences were significant ($p>0.05$). It is worth noting that these results were based on calculations from the treatment planning system, making them indicative rather than definite. The accuracy in dose well outside the treatment field is limited. Further measurement in the low dose region would be required in order to make any definitive conclusions about the difference in dose bath between flattened and unflattened beams.

A parameter that differed significantly between the different beam qualities was the complexity expressed as monitor units per delivered absorbed dose, MU/Gy, (Figure 11). The results were presented per dose (Gy) to allow comparison also between the conventional and the hypofractionated plans. The FFF plans required additional MU/Gy compared to standard plans, for both treatment arms. However, the MU/Gy for the C10FFF was not significantly larger than for the C10X. In practice an increase in MU/Gy implies an increase in treatment time. This effect is compensated by the increase in dose rate associated with removing the flattening filter. Depending on the degree of complexity and the available dose rate (related to photon energy), this is likely to counteract the additional MU/Gy and may even end up in decreasing the treatment time. In this study the increase in complexity is only a few percentages between the different beam qualities, while the increase in maximum dose rate between 10X and 10FFF is 400 %. This suggests that the increase in complexity on this level is not of clinical importance, which was indeed shown in the results from the measurements using the Delta^4. It is also in agreement with the results found by Gasic et al. (2014).

The majority of the plans fulfilled the dose constraints after the first optimization. There was however a few patients for which it was more challenging to meet the constraints, the rectum dose in particular. It is rather obvious that there will be a conflict in optimization between satisfactory target coverage and limited rectum dose, considering the rectum position being in proximity to the prostate and in

some cases even in contact with it. To investigate the correlation between plan complexity and the properties of the rectum, a structure defined as the overlap of PTV and rectum was introduced. It was found that there was a moderate, positive correlation between the size of the overlapping volume and complexity (Figure 12), implying that a larger overlap requires a more complex treatment plan. Unsurprisingly, the maximum value of the rectum diameter (at the level of the prostate) was found to be larger for the patients with a larger overlap in structures. Furthermore, a larger rectum diameter is associated with rectal filling. A full rectum has been shown more likely to induce prostate displacement (Ghilezan et al., 2005, Padhani et al., 1999). More specifically, Padhani with colleagues observed that patients with a rectum AP diameter > 37 mm were more prone to intra-fractional rectal movement, which may cause prostate displacements. In the currently on-going HYPO-RT-PC study the patients are not given any recommendations prior to initial scanning or treatment. However, according to the protocol the patients with a rectum diameter > 40 mm should be CT re-scanned before treatment planning.

To summarize the results of the dose distribution in the treatment plans, there is no significant difference in plan parameters between the different beam qualities. The treatment plans using FFF, 10 or 6 MV photons, generate not superior, but at least equal plans as standard 10 MV beams. This proves that it is feasible to generate VMAT treatment plans for extreme hypofractionation of prostate cancer using FFF-technique.

6.2 TREATMENT PLAN QUALITY: DELIVERY

Besides proving equal plan qualities, the aim of this study was to investigate if FFF could be used to decrease the treatment time for the hypofractionated deliveries. The beam-on time was measured for each of the treatments, delivered onto the Delta^4 pre-treatment verification phantom. The limitation to the standard beam and the 6 MV FFF lies in the dose rate. In some cases the modulation of the MLC might limit the gantry rotation, depending on the complexity of the segment. For the 10 MV FFF, the maximum available dose rate is 2400 MU/min. In this case, the gantry rotation becomes the limiting factor, which, due to safety regulations, is rotating at a maximum speed of one arc per minute. The decrease is still evident. Using 10 MV FFF, the treatment time of delivering 6.1 Gy/fraction is less than half the time of a standard 10 MV beam. These results are consistent with those by Zwahlen et al. (2012) and Gasic et al. (2014), both of which report significantly reduced treatment times with FFF.

This study differs from previous work in that the optimized plans were created with individual objectives for each plan to ensure clinically relevant treatment plans. Because of the request on decreasing treatment time for the hypofractionated cases from the clinic, it has been important to simulate the authentic clinical process through all the steps of the evaluation. Accordingly, all plans were verified through pre-treatment measurements using the dosimetry phantom Delta^4. Still, it was the final results of the evaluation that were of interest in this thesis work and not the specific objectives used during treatment planning.

The results from the gamma-evaluation showed that all treatment plans passed the clinical tolerance gamma criterion 3%, 2 mm. For the more stringent gamma criteria, the pass rate was observed to decrease with increasing stringency. The spread in pass rate was simultaneously increasing, which is expected. With stricter criteria smaller effects become prominent. The first points to fail were the field edges, due to high dose gradients. Also, with strong modulation within the fields it was generally the highest gradients that failed. The pass rate was acceptable down to 2%, 1 mm, indicating excellent delivery of the treatment plans. Only for gamma criterion 1%, 1 mm the majority of the plans had a pass rate below 90%. This is unlikely to have any clinical relevance for the patient.

No correlation between pass rate and prostate size (“small”, “medium” and “large”) was found. There seems to be no compromise in treatment delivery, despite variations in target size. Even the large prostate is a small enough target to be covered by the “flatter” central part of the FFF beam, making the profile very much alike the flattened beam. The correlation between pass rate and different

energies was also found to be non-significant in both treatment arms. Again, it is shown that it is feasible to deliver extreme hypofractionated radiotherapy for prostate cancer combining VMAT with FFF-technique. Other studies have shown similar results. Gasic et al. (2014) compared VMAT with and without flattening filter for five different types of tumours, one of them being prostate cancer. According to their results there was generally no significant dose difference in the treatment plans between the two techniques. They found the greatest benefit using FFF for small target volumes treated with high fractionation doses, significantly decreasing treatment times while maintaining plan quality. Alongi et al. (2013) gave a preliminary report of a phase II study on evaluating the safety of hypofractionated stereotactic body radiotherapy (SBRT) for prostate cancer using VMAT without flattening filter. The patients were treated with a schedule of 35 Gy in five fractions. The dosimetric evaluation showed that all dose-volume objectives were fulfilled for all patients. Preliminary results on outcome and toxicity implied that the FFF SBRT was feasible, delivering the treatment in approximately 2 minutes. Similarly, Ferrer Gonzalez et al. (2015) also showed that SBRT (35 Gy in five fractions) was feasible with VMAT FFF, but emphasised the need for longer follow up before any definite conclusions about late toxicity and outcome are possible.

There are recent publications describing the implementation of QA systems and gamma evaluation. For example, Arumugam et al. (2015) recommends a 2%, 2mm global gamma criterion combined with a minimum 85% pass rate for clinical verification of VMAT plans. The main limitation of the gamma method is that it only provides information about the percentage of points which fail the target criteria, and not the anatomical location in of these failures. Several groups have evaluated the performance of various available QA systems (Fredh et al. (2013), Coleman and Skourou (2013) and Nilsson et al. (2013)), the common finding being that it is often difficult to identify dosimetric errors using only a single gamma index. Recent developments in analysis have focussed more on comparing measured dosimetric deviations relative to anatomy and planned dose distribution. However, the ability to identify the errors also seems to depend on the treatment site and plan. Fredh et al. (2013) studied four different QA systems, including the Delta^4, evaluating four different IMRT plans with and without introduced errors. For the prostate case evaluated using the Delta4PT, all of the original plans had a pass rate >95%. Furthermore, the introduced errors of 3% dose deviation and 4 mm MLC error had the highest gamma failure rate. This implies that the system successfully identifies these types of errors. The Delta4 had the lowest failure rate for introduced collimator angle deviations of 2 and 5 degrees. However, in practice this is likely to have little dosimetric significance on a prostate cancer treatment.

In this study, all of the treatment plans showed pass rates >95% using gamma criterion 3%, 2mm. The gamma evaluation was performed on treatment plans generated for each individual patient using different beam qualities, thereby excluding any inter-patient dependence.

Using the applied method it is possible to relate the position of the failed voxels to the shape of the radiation field, which does in fact provide some information about the clinical relevance. However, due to the findings in other publications, it would be interesting to evaluate the results using DVHs and a visualized anatomical distribution, especially for the plans with a lower pass rate. This has been suggested as part of future perspectives of continued work on this study. The Delta4 software has a complementary module, where the measured dose distribution is recalculated using the patient's CT image set. The process was initiated during this thesis but due to limited time it was not possible to finish the implementation of the anatomical evaluation.

Finally, the method has been in clinical use in the department in Lund for several years now. Extensive QA of the Linacs is done on a monthly basis, e.g. on MLC performance. This in combination with the daily morning checks ensures accurate beam delivery. Thus, based on their experience, they conclude the gamma criterion 3%, 2mm with a pass rate of at least 90%, with further investigation if the pass rate is below 95%, to be adequate.

Based on the results of this, and previous, studies, VMAT combined with FFF-technique is realistic to implement at the department of Skåne University Hospital, as part of the HYPO-RT-PC study, without any additional work. Some of the TrueBeams are already operated in FFF-mode (6 MV) for other

treatments, such as stereotactic body radiotherapy for lung cancer. Introducing 10 MV FFF would require little effort. In the daily workflow it would imply checking the dose output for one additional energy, which in reality translates to approximately one or two minutes. The benefit of FFF VMAT for extreme hypofractionated radiotherapy is mainly the reduced treatment time, increasing patient comfort and possibly reducing the impact of prostate motion (which is further discussed in the next section). It may also be that the treatment delivery itself becomes more comparable to the conventional treatment if the required beam-on time is equal.

6.3 THE IMPACT OF PROSTATE MOTION

The final part of the study aimed to investigate the clinical relevance of prostate motion and what impact it may have on the treatment delivery. Results from previous publications emphasise the importance of reducing treatment time. Introducing VMAT as the main treatment technique instead of IMRT is one way of achieving this. However, in case of hypofractionation, the beam-on time is longer due to the higher absorbed dose delivered at each fraction. In this study, the treatment times are already shorter than in many previous trials but the hypothesis was that there may be larger uncertainties related to prostate displacement than necessary in the case of hypofractionated treatment plans using standard beams.

Several studies indicate an intra-fractional continuous drift in prostate position (Lovelock et al., 2015, Ballhausen et al., 2015, Langen et al., 2008). In the majority of patient cases, the displacements are small and covered by the CTV-PTV margins. However, the effect is still important to study as in the cases where it does occur it may affect the outcome of the treatment, also during shorter sessions. One study using continuous monitoring of the prostate suggests patient repositioning if the treatment duration exceeds 4-6 minutes (Cramer et al., 2013). Six different motion patterns of the prostate have been identified (Ng et al., 2012, Kupelian et al., 2007). Using trajectory data received from Ng et al, the effect of these motion patterns were investigated in this thesis through the delivery of two hypo-fractionated treatment plans, flattened and unflattened 10 MV (H10X and H10FFF, respectively).

The results of the stable trajectory (ST) and the continuous drift (CD) are the same as for the static delivery. This is expected, considering the offsets in these trajectories being small (less than 1 mm in the time frame of this study). This is also reassuring as the majority of patients are likely to exhibit this kind of motion. In the case of trajectories of persistent excursion (PE), high-frequency excursions (HE) and erratic behaviour (EB) the results from H10FFF are consistently better than for H10X; there is less difference in pass rate between H10FFF and the static delivery. The fact that the relative results are better for the unflattened beam is a direct effect of the shorter treatment delivery. It is not due to the properties of FFF beams, as it has already been shown in the previous part of the study that there is no significant difference in delivery or plan quality between flattened and unflattened 10 MV beams.

These results agree with the initial expectations of the study. The shorter delivery of the H10FFF means that the drift in position of the prostate is smaller, which is clearly seen in Figure 21 and 24. The pass rate decreases faster with increased stringency on the gamma criteria for a prostate in motion than the static case. Hence, decreasing the treatment time is preferable in all cases but transient excursion (TE). A short temporal displacement constitutes a larger fraction of the total dose delivery for H10FFF than for H10X, and is therefore expected to result in a slightly lower relative pass rate. However, it is worth noting that this is purely a difference in the number of points passing the gamma criterion and does not give any indication about the dosimetric or radiobiological effects. It would be of great interest to perform a DVH evaluation and get an anatomical evaluation of the results; although not achievable during the course of this thesis, it would be interesting for future perspectives.

Another interesting aspect is the correlation between prostate motion and rectal filling. The patients in the HYPO-RT-PC study are not given any instructions on emptying their rectum before treatment, but should be CT re-scanned if the rectum diameter exceeds 40 mm. There are studies clearly stating the

relation between rectal filling, causing rectal movements, and prostate intrafractional motion. The midpoint posterior on the prostate is the most critical point because of the rectal wall avoidance. Ghilezan et al. (2005) reported that for a full rectum, this anatomical point had a 10% probability of moving more than 3 mm in less than 1 minute compared to 20 minutes if the rectum was empty. Temporal displacements over 1 cm have been reported, where the motion appeared to be driven by peristalsis in the rectum, with a statistical significant difference observed between full and empty rectum (Mah et al., 2002).

Furthermore, decreasing the treatment time for the hypofractionated treatment may allow for a decrease in CTV-PTV margins in some patients, since the uncertainty in prostatic displacement is limited. Decreasing margins is likely to lead to reduced toxicity. In this study the CTV-PTV margin is set to 7 mm isotropically. This was decided at the beginning of the HYPO-RT-PC study when imaging quality was poor compared to today's techniques. Current set-up images are accurate and with daily verification of the prostate position it may be possible to introduce tighter margins if the treatment is delivered in 1 minute. For example, it has been shown that the required size of the margins is significantly smaller for treatment times of 2 minutes compared to 10 minutes (Shimizu et al., 2011). Further, the results by Gladwish et al. (2014) report less AP displacement for VMAT compared to fixed angle IMRT (longer treatment sessions), which they suggest is due to reduced uncertainties associated with random gaseous filling and emptying of rectum with reduced treatment time. Other studies suggest patient individual margins because of a large inter-patient spread in prostate displacements (Quon et al., 2012, Mutanga et al., 2011). Any conclusions about tighter margins are beyond the scope of this thesis project but it is an interesting aspect that should be further investigated.

7 CONCLUSIONS

In conclusion, flattening filter free volumetric modulated arc therapy for extreme hypofractionated prostate cancer may decrease treatment times below half the time for flattened beams with the same prescribed dose. Using 10 MV FFF, the time required to deliver 6.1 Gy in one arc is at the minimum achievable value of 1.0 minute. The plan quality and the quality of delivery are equal to those of flattened beams. Further, the fast treatment delivery limits the intra-fractional drift of the prostate and is advantageous in the majority of prostate motion trajectories investigated.

Finally, based on these results, it can be recommended to implement FFF VMAT for prostate cancer as part of the HYPO-RT-PC study at the department at Skåne University Hospital.

8 REFERENCES

ALONGI, F., COZZI, L., ARCANGELI, S., IFTODE, C., COMITO, T., VILLA, E., LOBEFALO, F., NAVARRIA, P., REGGIORI, G., MANCOSU, P., CLERICI, E., FOGLIATA, A., TOMATIS, S., TAVERNA, G., GRAZIOTTI, P. & SCORSETTI, M. 2013. Linac based SBRT for prostate cancer in 5 fractions with VMAT and flattening filter free beams: preliminary report of a phase II study. *Radiat Oncol,* 8**,** 171.

ARUMUGAM, S., YOUNG, T., XING, A., THWAITES, D. & HOLLOWAY, L. 2015. Benchmarking the gamma pass score using ArcCHECK for routine dosimetric QA of VMAT plans. *8th International Conference on 3D Radiation Dosimetry (IC3DDose)*. IOP Publishing.

BALLHAUSEN, H., LI, M., HEGEMANN, N. S., GANSWINDT, U. & BELKA, C. 2015. Intra-fraction motion of the prostate is a random walk. *Phys Med Biol,* 60**,** 549-63.

BOTH, S., WANG, K. K., PLASTARAS, J. P., DEVILLE, C., BAR AD, V., TOCHNER, Z. & VAPIWALA, N. 2011. Real-time study of prostate intrafraction motion during external beam radiotherapy with daily endorectal balloon. *Int J Radiat Oncol Biol Phys,* 81**,** 1302-9.

BRENNER, D. J. & HALL, E. J. 1999. Fractionation and protraction for radiotherapy of prostate carcinoma. *Int J Radiat Oncol Biol Phys,* 43**,** 1095-101.

CANCERFONDEN. 2014. *Prostatacancer* [Online]. Available: https://http://www.cancerfonden.se/om-cancer/prostatacancer.

CHUL-SEUNG, K. & YOUNG-NAM, K. 2013. *Curative Radiotherapy in Metastatic Disease: How to Develop the Role of Radiotherapy from Local to Metastases*.

COLEMAN, L. & SKOUROU, C. 2013. Sensitivity of volumetric modulated arc therapy patient specific QA results to multileaf collimator errors and correlation to dose volume histogram based metrics. *Med Phys,* 40**,** 111715.

CRAMER, A. K., HAILE, A. G., OGNJENOVIC, S., DOSHI, T. S., REILLY, W. M., RUBINSTEIN, K. E., NABAVIZADEH, N., NGUYEN, T., MENG, L. Z., FUSS, M., TANYI, J. A. & HUNG, A. Y. 2013. Real-time prostate motion assessment: image-guidance and the temporal dependence of intra-fraction motion. *BMC Med Phys,* 13**,** 4.

DASU, A. & TOMA-DASU, I. 2012. Prostate alpha/beta revisited -- an analysis of clinical results from 14 168 patients. *Acta Oncol,* 51**,** 963-74.

DZIERMA, Y., BELL, K., PALM, J., NUESKEN, F., LICHT, N. & RUBE, C. 2014. mARC vs. IMRT radiotherapy of the prostate with flat and flattening-filter-free beam energies. *Radiat Oncol,* 9**,** 250.

FERRER GONZALEZ, F., LETELIER, H., DE BLAS, R., BOLADERAS, A., PIÑEIRO, R., GALDEANO, M., SUAREZ, J. L., MARTINEZ, E., GUTIERREZ, C., PERA, J., PICON, C. & GUEDEA, F. 2015. EP-1258: Early experience in SBRT with VMAT and flattening filter free (FFF) beams. Phase I-II trial. *Radiother Oncol,* 115, Supplement 1**,** S680.

FOROUDI, F., TYLDESLEY, S., BARBERA, L., HUANG, J. & MACKILLOP, W. J. 2003. Evidence-based estimate of appropriate radiotherapy utilization rate for prostate cancer. *Int J Radiat Oncol Biol Phys,* 55**,** 51-63.

FREDH, A., SCHERMAN, J. B., FOG, L. S. & MUNCK AF ROSENSCHOLD, P. 2013. Patient QA systems for rotational radiation therapy: a comparative experimental study with intentional errors. *Med Phys,* 40**,** 031716.

GASIC, D., OHLHUES, L., BRODIN, N. P., FOG, L. S., POMMER, T., BANGSGAARD, J. P. & MUNCK AF ROSENSCHOLD, P. 2014. A treatment planning and delivery comparison of volumetric modulated arc therapy with or without flattening filter for gliomas, brain metastases, prostate, head/neck and early stage lung cancer. *Acta Oncol,* 53**,** 1005-11.

GEORG, D., KNOOS, T. & MCCLEAN, B. 2011. Current status and future perspective of flattening filter free photon beams. *Med Phys,* 38**,** 1280-93.

GHILEZAN, M. J., JAFFRAY, D. A., SIEWERDSEN, J. H., VAN HERK, M., SHETTY, A., SHARPE, M. B., ZAFAR JAFRI, S., VICINI, F. A., MATTER, R. C., BRABBINS, D. S. & MARTINEZ, A. A. 2005. Prostate gland motion assessed with cine-magnetic resonance imaging (cine-MRI). *Int J Radiat Oncol Biol Phys,* 62**,** 406-17.

GLADWISH, A., PANG, G., CHEUNG, P., D'ALIMONTE, L., DEABREU, A. & LOBLAW, A. 2014. Prostatic displacement during extreme hypofractionated radiotherapy using volumetric modulated arc therapy (VMAT). *Radiation Oncology,* 9.

HALL, E. J. & GIACCIA, A. J. 2006. *Radiobiology for the radiologist,* Philadelphia, Lippincott Williams & Wilkins.

KALANTZIS, G., QIAN, J., HAN, B. & LUXTON, G. 2012. Fidelity of dose delivery at high dose rate of volumetric modulated arc therapy in a truebeam linac with flattening filter free beams. *J Med Phys,* 37**,** 193-9.

KORREMAN, S., MEDIN, J. & KJAER-KRISTOFFERSEN, F. 2009. Dosimetric verification of RapidArc treatment delivery. *Acta Oncol,* 48**,** 185-91.

KUPELIAN, P., WILLOUGHBY, T., MAHADEVAN, A., DJEMIL, T., WEINSTEIN, G., JANI, S., ENKE, C., SOLBERG, T., FLORES, N., LIU, D., BEYER, D. & LEVINE, L. 2007. Multi-institutional clinical experience with the Calypso System in localization and continuous, real-time monitoring of the prostate gland during external radiotherapy. *Int J Radiat Oncol Biol Phys,* 67**,** 1088-98.

LANG, S., REGGIORI, G., PUXEU VAQUEE, J., CALLE, C., HRBACEK, J., KLOCK, S., SCORSETTI, M., COZZI, L. & MANCOSU, P. 2012. Pretreatment quality assurance of flattening filter free beams on 224 patients for intensity modulated plans: a multicentric study. *Med Phys,* 39**,** 1351-6.

LANGEN, K. M., WILLOUGHBY, T. R., MEEKS, S. L., SANTHANAM, A., CUNNINGHAM, A., LEVINE, L. & KUPELIAN, P. A. 2008. Observations on real-time prostate gland motion using electromagnetic tracking. *Int J Radiat Oncol Biol Phys,* 71**,** 1084-90.

LIN, Y., LIU, T., YANG, W., YANG, X. & KHAN, M. K. 2013. The non-Gaussian nature of prostate motion based on real-time intrafraction tracking. *Int J Radiat Oncol Biol Phys,* 87**,** 363-9.

LOVELOCK, D. M., MESSINEO, A. P., COX, B. W., KOLLMEIER, M. A. & ZELEFSKY, M. J. 2015. Continuous monitoring and intrafraction target position correction during treatment improves target coverage for patients undergoing SBRT prostate therapy. *Int J Radiat Oncol Biol Phys,* 91**,** 588-94.

LOW, D. A., HARMS, W. B., MUTIC, S. & PURDY, J. A. 1998. A technique for the quantitative evaluation of dose distributions. *Med Phys,* 25**,** 656-61.

MAH, D., FREEDMAN, G., MILESTONE, B., HANLON, A., PALACIO, E., RICHARDSON, T., MOVSAS, B., MITRA, R., HORWITZ, E. & HANKS, G. E. 2002. Measurement of Intrafractional Prostate Motion using Magnetic Resonance Imaging. *International Journal of Radiation Oncology Biology Physics,* 54**,** 568-575.

METCALFE, P., KRON, T., HOBAN, P. & METCALFE, P. 2007. *The physics of radiotherapy x-rays and electrons / by Peter Metcalfe, Tomas Kron, and Peter Hoban,* Madison, Wis., Medical Physics Pub.

MURRAY, L. J., THOMPSON, C. M., LILLEY, J., COSGROVE, V., FRANKS, K., SEBAG-MONTEFIORE, D. & HENRY, A. M. 2015. Radiation-induced second primary cancer risks from modern external beam radiotherapy for early prostate cancer: impact of stereotactic ablative radiotherapy (SABR), volumetric modulated arc therapy (VMAT) and flattening filter free (FFF) radiotherapy. *Phys Med Biol,* 60**,** 1237-57.

MUTANGA, T. F., DE BOER, H. C., VAN DER WIELEN, G. J., HOOGEMAN, M. S., INCROCCI, L. & HEIJMEN, B. J. 2011. Margin evaluation in the presence of deformation, rotation, and translation in prostate and entire seminal vesicle irradiation with daily marker-based setup corrections. *Int J Radiat Oncol Biol Phys,* 81**,** 1160-7.

NAHUM, A. E. 2015. The radiobiology of hypofractionation. *Clin Oncol (R Coll Radiol),* 27**,** 260-9.

NEDERVEEN, A. J., VAN DER HEIDE, U. A., DEHNAD, H., VAN MOORSELAAR, R. J., HOFMAN, P. & LAGENDIJK, J. J. 2002. Measurements and clinical consequences of prostate motion during a radiotherapy fraction. *Int J Radiat Oncol Biol Phys,* 53**,** 206-14.

NG, J. A., BOOTH, J., POULSEN, P. R., FLEDELIUS, W., WORM, E. S., EADE, T., HEGI, F., KNEEBONE, A., KUNCIC, Z. & KEALL, P. 2012. Kilovoltage Intrafraction Monitoring for Prostate Intensity Modulated Arc Therapy: First Clinical Results. *International Journal of Radiation Oncology Biology Physics,* 84**,** e655-61.

NILSSON, J., KARLSSON HAUER, A. & BÄCK, A. 2013. IMRT patient-specific QA using the Delta4 dosimetry system and evaluation based on ICRU 83 recommendations. *7th International Conference on 3D Radiation Dosimetry (IC3DDose)*. IOP Publishing.

OTTO, K. 2008. Volumetric modulated arc therapy: IMRT in a single gantry arc. *Med Phys,* 35**,** 310-7.

PADDICK, I. 2000. A simple scoring ratio to index the conformity of radiosurgical treatment plans. Technical note. *J Neurosurg,* 93 Suppl 3**,** 219-22.

PADHANI, A. R., KHOO, V. S., SUCKLING, J., HUSBAND, J. E., LEACH, M. O. & DEARNALEY, D. P. 1999. Evaluating the effect of rectal distension and rectal movement on prostate gland position using cine MRI. *Int J Radiat Oncol Biol Phys,* 44**,** 525-33.

PALMA, D. A., VERBAKEL, W. F., OTTO, K. & SENAN, S. 2010. New developments in arc radiation therapy: a review. *Cancer Treat Rev,* 36**,** 393-9.

QUON, H., LOBLAW, D. A., CHEUNG, P. C. F., HOLDEN, L., TANG, C., PANG, G., MORTON, G., MAMEDOV, A. & DEABREU, A. 2012. Intra-fraction Motion during Extreme Hypofractionated Radiotherapy of the Prostate using Pre- and Post-treatment Imaging. *Clinical Oncology,* 24**,** 640-5.

SHELTON, J., ROSSI, P. J., CHEN, H., LIU, Y., MASTER, V. A. & JANI, A. B. 2011. Observations on prostate intrafraction motion and the effect of reduced treatment time using volumetric modulated arc therapy. *Pract Radiat Oncol,* 1**,** 243-50.

SHIMIZU, S., OSAKA, Y., SHINOHARA, N., SAZAWA, A., NISHIOKA, K., SUZUKI, R., ONIMARU, R. & SHIRATO, H. 2011. Use of Implanted Markers and Interportal Adjustment with Real-time Tracking Radiotherapy System to Reduce Intrafraction Prostate Motion. *International Journal of Radiation Oncology Biology Physics,* 81**,** e393-399.

SLOTMAN, B. J., COTTIER, B., BENTZEN, S. M., HEEREN, G., LIEVENS, Y. & VAN DEN BOGAERT, W. 2005. Overview of national guidelines for infrastructure and staffing of radiotherapy. ESTRO-QUARTS: work package 1. *Radiother Oncol,* 75**,** 349-54.

STATHAKIS, S., ESQUIVEL, C., GUTIERREZ, A., BUCKEY, C. R. & PAPANIKOLAOU, N. 2009. Treatment planning and delivery of IMRT using 6 and 18MV photon beams without flattening filter. *Appl Radiat Isot,* 67**,** 1629-37.

SWEDISH NATIONAL HEALTH CARE PROGRAMME FOR PROSTATE CANCER. 2015.

THARIAT, J., HANNOUN-LEVI, J. M., SUN MYINT, A., VUONG, T. & GERARD, J. P. 2013. Past, present, and future of radiotherapy for the benefit of patients. *Nat Rev Clin Oncol,* 10**,** 52-60.

TONG, X., CHEN, X., LI, J., XU, Q., LIN, M., CHEN, L., PRICE, R. A. & MA, C. 2015. Intrafractional prostate motion during external beam radiotherapy monitored by a real-time target localization system. *Journal of Applied Clinical Medical Physics,* 16.

VARIAN MEDICAL SYSTEMS, I. 2011. Eclipse Algorithms Reference Guide.

VASSILIEV, O. N., KRY, S. F., CHANG, J. Y., BALTER, P. A., TITT, U. & MOHAN, R. 2009. Stereotactic radiotherapy for lung cancer using a flattening filter free Clinac. *Journal of Applied Clinical Medical Physics,* 10**,** 14-21.

WIDMARK, A., FRANZÉN, L., HALL, E., DEARNALEY, D., GUNNLAUGSSON, A. & NILSSON, P. 2014. *ISRCTN: Phase III study of HYPO-fractionated radiotherapy of intermediate risk localised prostate cancer.* [Online]. Available: http://www.controlled-trials.com/ISRCTN45905321.

WILLIAMS, S. G., TAYLOR, J. M., LIU, N., TRA, Y., DUCHESNE, G. M., KESTIN, L. L., MARTINEZ, A., PRATT, G. R. & SANDLER, H. 2007. Use of individual fraction size data from 3756 patients to directly determine the alpha/beta ratio of prostate cancer. *Int J Radiat Oncol Biol Phys,* 68**,** 24-33.

WILLOUGHBY, T. R., KUPELIAN, P. A., POULIOT, J., SHINOHARA, K., AUBIN, M., ROACH, M., 3RD, SKRUMEDA, L. L., BALTER, J. M., LITZENBERG, D. W., HADLEY, S. W., WEI, J. T. & SANDLER, H. M. 2006. Target localization and real-time tracking using the Calypso 4D localization system in patients with localized prostate cancer. *Int J Radiat Oncol Biol Phys,* 65**,** 528-34.

WOLFF, D., STIELER, F., WELZEL, G., LORENZ, F., ABO-MADYAN, Y., MAI, S., HERSKIND, C., POLEDNIK, M., STEIL, V., WENZ, F. & LOHR, F. 2009. Volumetric modulated arc

therapy (VMAT) vs. serial tomotherapy, step-and-shoot IMRT and 3D-conformal RT for treatment of prostate cancer. *Radiother Oncol,* 93**,** 226-33.

YU, C. X. 1995. Intensity-modulated arc therapy with dynamic multileaf collimation: an alternative to tomotherapy. *Phys Med Biol,* 40**,** 1435-49.

ZELEFSKY, M. J., KOLLMEIER, M., COX, B., FIDALEO, A., SPERLING, D., PEI, X., CARVER, B., COLEMAN, J., LOVELOCK, M. & HUNT, M. 2012. Improved clinical outcomes with high-dose image guided radiotherapy compared with non-IGRT for the treatment of clinically localized prostate cancer. *Int J Radiat Oncol Biol Phys,* 84**,** 125-9.

ZWAHLEN, D. R., LANG, S., HRBACEK, J., GLANZMANN, C., KLOECK, S., NAJAFI, Y., STRELLER, T., STUDER, G., ZAUGG, K. & LUETOLF, U. M. 2012. The use of photon beams of a flattening filter-free linear accelerator for hypofractionated volumetric modulated arc therapy in localized prostate cancer. *Int J Radiat Oncol Biol Phys,* 83**,** 1655-60.